PNAS
www.pnas.org

## Supplementary Information for

# "Morphological, cellular and molecular basis of brain infection in COVID-19 patients"

**Fernanda Crunfli[1#], Victor Corasolla Carregari[1#], Flavio P. Veras[2#],** Lucas Scardua Silva[1], Mateus Henrique Nogueira[1], André Saraiva Leão Marcelo Antunes[1], Pedro Henrique Vendramini[1], Aline Gazzola Fragnani Valença[1], Caroline Brandão-Teles[1], Giuliana da Silva Zuccoli[1], Guilherme Reis-de-Oliveira[1], Lícia C. Silva-Costa[1], Verônica Monteiro Saia-Cereda[1], Bradley J Smith[1], Ana Campos Codo[1], Gabriela F de Souza[1], Stéfanie P Muraro[1], Pierina Lorencini Parise[1], Daniel A. Toledo-Teixeira[1], Ícaro Maia Santos de Castro[3], Bruno Marcel Melo[2], Glaucia M. Almeida[2], Egidi Mayara Silva Firmino[2], Isadora Marques Paiva[2], Bruna Manuella Souza Silva[2], Rafaela Mano Guimarães[2], Niele D. Mendes[2], Raíssa Guimarães Ludwig[1], Gabriel P. Ruiz[1], Thiago Leite Knittel[1], Gustavo G Davanzo[1], Jaqueline Aline Gerhardt[1], Patrícia Brito Rodrigues[1], Julia Forato[1], Mariene Ribeiro Amorim[1], Natália Brunetti Silva[1], Matheus Cavalheiro Martini[1], Maíra Nilson Benatti[2], Sabrina S Batah[2], Li Siyuan[2], Rafael Batista João[1], Ítalo Karmann Aventurato[1], Mariana Rabelo de Brito[1], Maria Julia Mendes[1], Beatriz Amorim da Costa[1], Marina KM Alvim[1], José Roberto da Silva Júnior[1], Lívia Liviane Damião[1], Iêda Maria Pereira de Sousa[1], Elessandra Dias da Rocha[1], Solange Maria Gonçalves[1], Luiz Henrique Lopes da Silva[1], Vanessa Bettini[1], Brunno M Campos[1], Guilherme Ludwig[1], Lucas Alves Tavares[2], Marjorie Cornejo Pontelli[2], Rosa Maria Mendes Viana[2], Ronaldo B Martins[2], Andre Schwambach Vieira[1], José Carlos Alves-Filho[2], Eurico Arruda[2], Guilherme Gozzoli Podolsky-Gondim[2], Marcelo Volpon Santos[2], Luciano Neder[2], André Damasio[1], Stevens Rehen[4,5], Marco Aurélio Ramirez Vinolo[1] Carolina Demarchi Munhoz[3], Paulo Louzada-Junior[2], Renê Donizeti Oliveira[2], Fernando Q. Cunha[2], Helder I Nakaya[3], Thais Mauad[3], Amaro Nunes Duarte-Neto[3], Luiz Fernando Ferraz da Silva[3], Marisa Dolhnikoff[3], Paulo Hilario Nascimento Saldiva[3], Alessandro S. Farias[1], Fernando Cendes[1], Pedro Manoel M. Moraes-Vieira[1], Alexandre T. Fabro[2], Adriano Sebollela[2], José L Proença-Modena[1], **Clarissa Lin Yasuda[1*], Marcelo A Mori[1*], Thiago Mattar Cunha[2*], Daniel Martins-de-Souza[1,4*].**

1- University of Campinas (UNICAMP), Campinas, São Paulo, Brazil;
2- Ribeirão Preto Medical School (FMRP), University of São Paulo (USP), Ribeirão Preto, São Paulo, Brazil;
3- University of São Paulo (USP), São Paulo, Brazil;
4- D'Or Institute for Research and Education (IDOR), Brazil;
5- Institute of Biomedical Science (ICB), Federal University of Rio de Janeiro (UFRJ), Rio de Janeiro, Brazil;

**# These authors contributed equally to this work.**

***Correspondence should be addressed to:**

**Daniel Martins-de-Souza, PhD:** dmsouza@unicamp.br

**Thiago Mattar Cunha, PhD:** thicunha@fmrp.usp.br

**Marcelo A. Mori, PhD:** morima@unicamp.br

**Clarissa Lin Yasuda, MD, PhD:** cyasuda@unicamp.br

Supplementary text - Materials and methods Figures S1 to S13
Tables S1 to S7
SI References

## Supplementary Information Text

### Materials and methods

***Brain imaging and neuropsychological evaluation***

### Participants

Eighty-one patients (61 women, median 36 years of age) previously infected with SARS-CoV-2 were enrolled prospectively for this study after signing an informed consent form approved by the local ethics committee. These individuals were diagnosed during the first semester of 2020, presented mild symptoms during the acute phase, and did not require hospitalization or oxygen therapy. There was a median interval of 54 days (range 16-120 days) between their RT-PCR exam and the day of MRI scanning and interview. The outpatients and healthy controls were balanced for age ($p=0.97$) and sex ($p=0.3$). Epidemiological and clinical data are displayed in Table S1. Patients and healthy volunteers were recruited from the same environment; they were workers and students from the university campus and citizens from the community around the campus. We advertised the study in the university newsletters and used advertisements around the campus. The neuroimaging analyses and subsequent neuropsychological evaluations were approved by the Research Ethics Committee of the University of Campinas (CAAE: 31556920.0.0000.5404) and all subjects signed a consent form to participate.

**Neuropsychological evaluation**

We performed neuropsychological evaluations of the patients who underwent MRI scanning, 61 agreed to stay for neuropsychological evaluation on the same day. They were tested for symptoms of anxiety using the Beck Anxiety Inventory (BAI) and symptoms of depression using the Beck Depression Inventory (BDI-II) (1). Anxiety symptoms were considered present when the BAI was higher than 10 points, and depression symptoms were considered present when the BDI-II was 14 points or higher. Anxiety symptoms were classified as mild (BAI 11-19), moderate (20-30), or severe (31-63); and depression symptoms were classified as mild (BDI 14-19), moderate (20-35) or severe (36-63). We evaluated episodic verbal memory (immediate and delayed recall) using the Logical Memory subtest from the Wechsler Memory Scale (WMS-R) (2), in which the examiner verbally presents two stories, each including 25 pertinent pieces of information. Subjects are required to recall details of each story immediately after its presentation and again after 20 minutes. We administered the Color Trails Test (CTT) to evaluate other cognitive functions (3). The CTT is subdivided into two steps: *Step A* assesses sustained attention, processing speed, and visual search in a task that requires connecting 25 randomly arranged numbers in ascending order; *Step B* evaluates alternating attention and cognitive flexibility in a task associated with shifting rules in an ascending sequence of 25 numbers. A training stage was applied to both steps. We calculated z-scores for the results of these tests based on Brazilian normative data (2, 4). We controlled for the effects of age or education in a separate analysis using multiple linear regression residuals when the normative data covered only one of these variables. For each test, the function was categorized as preserved (asymptomatic individuals) for z-scores $\geq$ -0.99 (including average, high average, above average, and exceptionally

high scores); cognitive impairments were defined for z-scores ≤ -1, and were classified as mild (low-average; z-score between -1 and -1.5), moderate (below-average; z-score between -1.51 and -2), or severe (exceptionally low; z-score < -2). The Chalder Fatigue Questionnaire (CFQ-11) (5) was used to evaluate fatigue. Individuals were instructed to answer 11 questions (measured on a Likert scale of 0-3), which yields a global score out of 33. To quantify excessive daytime sleepiness, we administered the Epworth Sleepiness Scale (ESS), a self-reported questionnaire with eight situations involving daily activities. The global scores range from 0 to 24; the diagnosis of EDS was suggested for those with scores higher than 10 (6). We used SPSS 22 and R-software (http://www.R-project.org/) (7) for statistical analyses of clinical and neuropsychological variables. Results are illustrated in Table S2.

**Neuroimaging analysis**

We obtained the structural, 3D, T1-weighted images using a 3T Philips-Achieva MRI scanner (voxel size: 1x1x1 $mm^3$, TE = 3.2 ms, TR = 7 ms, matrix = 240x240x180, flip angle = 8, and FOV = 240x240 $mm^2$) (1, 8) for COVID-19 patients and controls. We performed imaging analyses with the CAT12 toolbox (http://www.neuro.uni-jena.de/cat/, version r1932 13th January 2022) within SPM12 (http://www.fil.ion.ucl.ac.uk/spm/, version 7771) running on MATLAB 2019b to extract Cortical Thickness (CT) maps, according to the default parameters. The T1 images were first spatially registered and segmented into gray matter, white matter, and cerebrospinal fluid before calculating cortical thickness using the projection method described by Dahnke *et al.* (9). For statistical analyses of extracted maps, we used CAT12/SPM12 tools to parcellate the individual maps into regions of interest (10) and subsequently performed an ANOVA 5

(comparing COVID-19 patients and healthy controls), including age and sex as covariates. We applied the Holm-Bonferroni method to correct for multiple comparisons.

***Correlations between neuropsychological scores and cortical thickness***

We investigated possible associations between neuropsychological scores and cortical thickness. We hypothesized that elevated fatigue levels could impair cognitive performance (11) and be associated with anxiety levels (12). Therefore, we tested the relationship between fatigue scores and the neuropsychological scores of interest. There were correlations between fatigue and immediate logical memory ($r=-0.32$; $p=0.03$) fatigue and Color Trail B ($r=-0.3$; $p=0.04$), and fatigue and anxiety ($r=0.46$; $p=0.001$). These correlations between neuropsychological scores and cortical thickness were adjusted for fatigue with partial correlations, calculated in an R environment (using the cor.test function on the partial residuals), which provided the confidence intervals (the asymptotic 95% CI for median values and 95% CI for correlations). The false discovery rate (FDR) (13) was utilized to adjust p-values for multiple comparisons in R (7). The results are presented in Table S3.

***Postmortem brain samples from COVID-19***

Twenty-six individuals who died from complications related to COVID-19 were autopsied with an ultrasound-guided, minimally invasive approach using endonasal trans-ethmoidal access, performed within 1 hour of the patient's death. Brain tissue samples collected and fixed using a 10% neutral buffered formalin solution. After fixation, the tissue was embedded in a paraffin block and sectioned into 3μm slices. The sections were stained by H&E and immunofluorescence was observed. For the proteomic analysis,

twelve COVID-19 patients were autopsied using the same approach and the samples were frozen at -80°C. Brain tissue samples were macerated in lysis buffer (100mM Tris-HCl, pH 8.0, 150mM NaCl, 1mM EDTA, 0.5% Triton X-100) prior to trypsin digestion. The clinical data of all COVID-19 patients and control patients are described in Table S4, S5, S6, and S7. The autopsy studies were approved by the National Commission for Research Ethics (CAAE: 32475220.5.0000.5440 and CAAE: 38071420.0.1001.5404).

***Generation of human astrocytes (hES-derived)***

Differentiation of glial progenitor cells was performed from neural stem cells (NSC) derived from pluripotent human embryonic stem cells (hES, BR-1 cell line) (14), according to the method published by Trindade, 2020 (15). NSCs were cultured in plates coated with Geltrex Matrix (Thermo Fisher Scientific, MA, USA) using 1:1 Neurobasal™/Advanced DMEM/F12 medium and 2% neural induction supplement. Upon reaching 50% confluence, the medium was changed to DMEM/F12 (Dulbecco's Modified Eagle Medium/F12), 1% N2 supplement, 1% fetal bovine serum (FBS) and 1% penicillin-streptomycin, and the plates were maintained at 37°C in humidified air with 5% $CO_2$ for 21 days. At this stage, cells were considered glial progenitor cells (GPCs). Subsequently, GPCs were plated at low density (30-40% confluence) on Geltrex-coated plates and treated with DMEM/F12 medium, 1% GlutaMAX Supplement, 10% FBS and 1% penicillin-streptomycin. The differentiation medium was replaced every 2-3 days. After 4 weeks of differentiation, the cells were considered mature astrocytes. These cells were plated on Geltrex-coated coverslips at a density of $4x10^4$ cells per well for immunostaining assays (24-well plates) and $2.5x10^5$ cells per well for viral load and proteomic and metabolomic analysis (6-well plates). All products used for cell culture are from Thermo Fisher

Scientific, MA, USA. The characterization of the BR-1 lineage as astrocyte cells has been previously described elsewhere (14–17). We generated eight batches of human astrocytes from BR-1-derived NSCs. The NSCs were of different passages and were used as biological replicates in independent experiments. Our internal control showed that about 97% of the neural stem cell-derived astrocytes in culture expressed GFAP, 80.4% expressed vimentin and 12.9% expressed SOX-2 (markers of progenitor cells). The neural stem cell-derived astrocyte culture expressed more astrocytic markers than progenitor cell markers, showing an excellent effectiveness of human astrocyte generation (Fig. S12).

***Virus strain***

The HIAE-02-SARS-CoV-2/SP02/human/2020/BRA virus strain (GenBank accession number MT126808.1) was used for all *in vitro* experiments. The virus was isolated from the first confirmed case of COVID-19 in Brazil and was kindly donated by Prof. Dr. Edison Durigon (ICB-USP). The replication-competent pseudotyped vesicular stomatitis virus with the full-length SARS-CoV-2 spike protein replacing the virus glycoprotein gene, and containing an eGFP reporter (VSV-eGFP-SARS-CoV-2) was engineered and donated by Prof. Dr. Sean P.J. Whelan (Department of Medicine, Washington University School of Medicine, St. Louis, MO, USA) for SARS-CoV-2 entry experiments (18). Viral stock was propagated in Vero CCL-81 cells (ATCC), cultivated in DMEM supplemented with 10% heat-inactivated FBS and 1% penicillin and streptomycin (Gibco, Walthmam, MA, USA) and incubated at 37°C with 5% atmospheric $CO_2$. Viral titer was determined by the plaque-forming assay using Vero cells.

***In vitro infection***

Astrocytes were infected with SARS-CoV-2 for 1h using an MOI of 0.1 (proteomics; metabolomics; gene expression, viral load and bioenergetics assays; and flow cytometry analysis) or 1.0 (proteomics and immunostaining) under gentle agitation at room temperature. After viral adsorption, cells were washed twice with phosphate-buffered saline (PBS) and incubated with DMEM/F12 supplemented with 10% FBS, 1% GlutaMAX and 1% penicillin and streptomycin for 24h at standard culture conditions (37ºC and 5% atmospheric $CO_2$). SARS-CoV-2 entry experiments were performed using SARS-CoV-2 (MOI 1.0) and VSV-eGFP-SARS-CoV-2 pseudotyped particles (MOI 1.0) in the presence of an NRP1-neutralizing antibody (BD Bioscience, Cat. 743129, Clone U21-1283). We used anti-IgG2b as a control antibody (Biolegend, Cat. 406703, Clone RMG2b-1).

***Single-nucleus transcriptomic analysis***

We analyzed publicly available single-nucleus transcriptome data from the medial frontal cortices of 8 patients (4 non-viral controls and 4 patients with COVID-19). The data was generated by Yang et al. (19) and made publicly available at https://twc-stanford.shinyapps.io/scRNA_Brain_COVID19. The dataset was downloaded and the RDS file was imported into R environment version v3.6.3. Astrocytes were filtered based on cell type annotations provided by the original authors. To calculate the percentage of cells expressing BSG and NRP1, cell frequency was calculated considering cells with gene count ≥ 1 in the RNA essay for each gene (BSG and NRP1). Cells that met this criterion of minimum expression were considered as expressing the respective gene. A differential expression analysis was conducted using the FindMarkers function in Seurat with the

Wilcoxon test comparing COVID-19 astrocyte cells vs. non-viral astrocyte cells. To investigate reactive astrogliosis markers, astrocyte cells were filtered based on the authors' cell annotations and re-clustered with Seurat v.3 (20) Briefly, the data matrix was normalized using the SCTransform method in Seurat v.3 with default parameters. Variables 'nCount_RNA' and 'percent.mito' were regressed out in the scaling step and a PCA was performed using the top 3,000 variable genes. Then, UMAP and tSNE were performed on the top 10 principal components for visualizing the cells. Graph-based clustering was performed on the PCA-reduced data using the Louvain method with a resolution of 0.4. Based on this approach, 8 clusters of astrocyte cells were identified. Genes were calculated considering a minimum cellular gene expression of 5% and average log fold change above 0.1. The differential expression analysis was conducted using the FindMarkers function in Seurat with the Wilcoxon test comparing COVID-19 cells *vs.* non-viral cells. Genes were considered differentially expressed if the adjusted p-value was below 0.05.

***Immunostaining and confocal microscopy***

Brain sections from autopsies and astrocyte cell cultures were fixed with 10% neutral buffered formalin solution or 4% paraformaldehyde (PFA), respectively. Subsequently, the samples were incubated with primary antibodies: mouse monoclonal anti-GFAP Alexa Fluor 488 (EMD Millipore, clone GA5, Cat. MAB3402X, 1:400), human chimeric monoclonal anti-SARS-CoV-2 spike S1 (GeneScript, clone HC2001, Cat. A02038, 1:500), rabbit polyclonal anti-SARS-CoV-2 spike (Rhea Biotech, Cat. IM-0828, 1:200), rabbit monoclonal anti-SARS-CoV-2 Spike (Invitrogen, clone T01KHuRb, Cat. 703959, 1:500), mouse monoclonal anti-double stranded RNA J2 (dsRNA, SCICONS

English & Scientific Consulting Kft., clone J2-1909, Cat. 10010200; 1:1,000), rabbit polyclonal anti-IBA1 (FUJIFILM Wako Pure Chemical Corporation, Cat. 019-19741, 1:1,000) and rabbit monoclonal anti-NeuN (Abcam, clone EPR12763, Cat. Ab128886, 1:1,000). The slides were washed twice with TBS-T (Tris-Buffered Saline with Tween 20) and incubated with secondary antibodies donkey anti-mouse IgG AlexaFluor 647 (Thermo Fisher Scientific; Cat. A32787; 1:800) or AlexaFluor 488 (Abcam; Cat. ab150061; 1:800), donkey anti-rabbit IgG AlexaFluor 488 (Abcam; Cat. ab150065; 1:800) or AlexaFluor 594 (Abcam; Cat. ab150076; 1:800) and goat anti-human IgG FITC (Rhea Biotech, Cat. IC-3H04, 1:400). Controls were performed for secondary antibody fluorescence. Antibodies for detecting SARS-CoV-2 in human brain tissue and human astrocytes *in vitro* were first validated with SARS-CoV-2-infected and non-infected Vero cells. In addition, we validated the antibodies in brain sections from controls.

Nuclei were stained with DAPI (Life Technologies; Cat. D1306; 1:1,000). Images were acquired by an Axio Observer combined with an LSM 780 confocal device (Carl Zeiss) with 630x magnification and Z-stack (0.15µm) for brain sections. Colocalization analyses between GFAP and SARS-CoV-2 S1 or GFAP and dsRNA were quantified using Fiji/ImageJ software (21). To determine colocalization, we used a ratio of GFAP:SARS-CoV-2 and GFAP:dsRNA in each sample by analyzing Pearson's correlation coefficients.

***Western blots***

Astrocytic cell culture samples were collected in RIPA Buffer (Sigma Aldrich, Cat. R0278) with protease and phosphatase inhibitors (Cell Signaling, Cat. 5872S). Protein content was quantified using a BCA protein assay kit (Sigma Aldrich, Cat. BCA1). Extracts

were separated by 10% SDS-PAGE and transferred to nitrocellulose membranes. After transfering, the membranes were incubated at 4ºC with blocking buffer for 2h. The membranes were incubated in 5% BSA solution (Sigma Aldrich, Cat. A7906) and 0.1% Tween 20 (Sigma Aldrich, Cat. P2287) containing rabbit anti-ACE2 polyclonal antibody (Abcam; Cat. ab15348; 1:2,000) or rabbit anti-NRP1 monoclonal antibody (Abcam; clone EPR3113 Cat. ab81321; 1:1,000) overnight at 4ºC. Next, the membranes were incubated with anti-rabbit polyclonal antibody (Invitrogen; Cat. 31460; 1:5,000) for 1h. Finally, membranes were incubated with anti-beta-actin (Cell Signaling; clone 8H10D10; Cat. 3700) for 2h at room temperature. Beta-actin expression was used as loading control and was incubated post-ACE2/NRP1 without a stripping process. Fluorescence was detected with an ECL system (Millipore, Cat. WBULS0500) and Chemidoc imaging system (Bio-Rad Laboratories).

***Human brain slice cultures***

Cultures were prepared as previously described (22, 23). Temporal lobe resections were obtained from two patients who underwent surgery to remove a hippocampal epileptic focus. Collected tissue corresponds to a non-epileptogenic area removed to provide access to the structures to be resected. In our previous works involving adult human brain-derived slice cultures, we have shown the presence of neurons, microglia and astrocytes with no significant morphological/cytoarchitectural alterations, including the preservation of all neuronal cortical layers (22, 23). Tissue was collected in the surgery room immediately after resection and transported to the laboratory, where it was sliced at 200 μm in a VT1000s automatic vibratome (Leica) and cultivated free-floating with Neurobasal A (Gibco) medium supplemented with 1% Glutamax (Gibco), 1% penicillin/streptomycin

(Gibco), 2% B27 (Gibco) and 0.25µg/mL fungizone (Sigma). This procedure was approved by the Ethics Committee of the Ribeirao Preto Medical School (HCRP protocol #17578/15). For viral infection, the medium was removed, and the slices were exposed to a TCID50 of $3x10^6$ for SARS-CoV-2 or an equivalent volume of mock medium. Infection was performed for 2h at 37°C and 5% $CO_2$ in a biosafety level 3 laboratory. The inoculum was removed, the tissue was washed and the slices were maintained in fresh medium at 37°C and 5% $CO_2$ until processing for subsequent analysis.

***Proteomics sample preparation, LC-MS/MS analyses and data processing***

Astrocytes infected with SARS-CoV-2 and a mock control were collected in biological triplicate. Cells were chemically lysed with lysis buffer (100mM Tris-HCl, 1mM EDTA, 150mM NaCl, 1% Triton-X and protease and phosphatase inhibitors) and mechanically lysed with an ultrasonication probe during 3 cycles of 20s each with 90% frequency on ice. The total protein extract was quantified by BCA, according to the manufacturer's instructions (Thermo Fisher Scientific, MA, USA). 30µg of total protein extract from each sample was transferred to a Microcon-10 centrifugal filter with a 10kDa cutoff for FASP protein digestion (24). Proteins were reduced (10mM DTT) at 56°C for 40min, alkylated by 20min in dark at a room temperature (50mM IAA) and digested overnight by trypsin at 37°C in 50mM ammonium bicarbonate (AmBic), pH 8.0. On the following day, the peptides were recovered from the filter in 50mM AmBic, and trypsin activity was quenched by adding formic acid (FA) to a final concentration of 1% (v/v), whereupon the peptides were desiccated in a SpeedVac and stored at -80°C until use.

Digested peptides were resuspended in 0.1% FA. LC-MS/MS analyses were performed in an ACQUITY UPLC M-Class System (Waters Corporation, Milford, MA) coupled online to a Synapt G2-Si mass spectrometer (Waters Corporation, Milford, MA). 1µg of peptides were loaded onto a trapping column (Symmetry C18 5µm, 180µm × 20mm, Waters Corporation, Milford, MA) and subsequently separated in the analytical column (HSS T3 C18 1.8µm, 75µm × 150mm; Waters Corporation, Milford, MA). For gradient elutions, 0.1% FA was used as solvent A and acetonitrile-FA (99.9% ACN:0.1% FA) as solvent B. A reversed phase gradient was carried out during a 120-minute method, with a linear gradient of 3 - 60% acetonitrile over 90min at 300nL/min. In the Synapt G2-Si, the peptide spectra were acquired by ion mobility-enhanced data-independent acquisition ($HDMS^E$). Mass spectrometry analysis was performed in "Resolution Mode", switching between low (4eV) and high (25–60eV) collision energies, using a scan time of 1.0s per function over 50–2000m/z. The wave velocity for ion mobility separation was 1,000m/s and the transfer wave velocity was 175m/s. A [Glu1]-Fibrinopeptide B standard (Waters Corporation, Milford, MA) was used as the reference lock-mass compound. Each sample was run in three technical replicates.

The raw data from each experiment were processed in Progenesis QI for Proteomics (version 4.0; Waters Corporation, Milford, MA). Tandem mass spectra were searched against the *Homo sapiens* proteome database (UNIPROT, reviewed, release 2020-04), using tolerance parameters of 20ppm for precursor ions and 10ppm for product ions. For peptide identification, carbamidomethylation of cysteines was set as a fixed modification and oxidation of methionines as a variable modification, 2 missed cleavages were permitted and the false discovery rate (FDR) was limited to 1%. Protein identification was performed

using a minimum of 1 fragment ion matched per peptide, a minimum of 3 fragment ions per protein and a minimum of 1 peptide per protein.

The label-free quantitative analysis was carried out using relative abundance intensity, normalized by all identified peptides. The expression analysis was performed considering the technical replicates for each experimental condition, following the hypothesis that each group is independent. Proteins with ANOVA ($p$) $\leq 0.05$ between groups were considered differentially expressed.

***Bioinformatic analyses***

Proteomic data visualization was performed in-house in Python (v. 3.7.3). Differentially regulated proteins ($p \leq 0.05$) were submitted to systems biology analysis in R (v. 4.0) and Cytoscape environments (25). While performing the over-representation analysis (ORA), proteins were enriched using the ClusterProfiler R package (26), CellMarker Database (27) and Kyoto Encyclopedia of Genes and Genomes (KEGG) (28). The network analysis was run as a Reactome Cytoscape plugin (29) for module detection and pathway enrichment analysis.

***Metabolomics sample preparation, UPLC-MS/MS analyses, and data processing***

Astrocytes were washed twice with PBS at physiological pH, then the cells were collected with 600µL of methanol. Samples were dried and stored at -80°C until the metabolite extraction step. 473µL of water, 600µL of methanol and 1168µL of chloroform were added and the tubes were shaken vigorously for 2 minutes. Subsequently, samples were centrifuged for 5min at 13,000 x*g*. The aqueous supernatant and the organic phase

(lower phase) were collected and dried for 60min and 40min, respectively, in a vacuum concentrator. All samples were stored at -80°C until analysis by LC-MS/MS.

The samples were resuspended in 100µL of a methanol:water mixture (1:1) and for each analysis, 4µL of the sample was injected. Sample separation was performed by hydrophobic interaction liquid chromatography (HILIC) using an Acquity UPLC® BEH amide column (1.7µm, 2.1mm x 100mm). The mobile phases used for the separations were ACN:$H_2O$ (80:20) as mobile phase A and ACN:$H_2O$ (30:70) as mobile phase B, both phases containing 10mM ammonium formate and 0.1% ammonium hydroxide. Separation was then performed by a gradient from 99 - 1% buffer A over 7min. The column was returned to 99% buffer A for 2min for re-equilibration before the next injection for a total run time of 10min. Data acquisition was performed in negative mode and the instrument was operated in $MS^E$ mode in the m/z range of 50–800Da, with an acquisition time of 0.1s per scan.

Identification of the metabolites of interest was carried out manually by spectral features, and the level 3 identification was obtained according to Schrimpe-Rutledge et al. (30) using 5ppm as the error cutoff. The integration area of each peak was used to calculate the violin plot and an unpaired t-test with Welch's correction was used for statistical comparison. All analyses were performed using GraphPad Prism 8.0 software (San Diego, CA, USA) and a significance level of $p \leq 0.05$ was adopted.

***RNA extraction, gene expression analyses and viral load***

Total RNA extraction was performed using TRI Reagent according to the manufacturer's instructions (Sigma, St Louis, USA). RNA concentration was determined

by a DeNovix spectrophotometer and RNA integrity was assessed by visualization of 28S and 18S ribosomal RNA on a 1% agarose gel. Reverse transcription was performed with 0.5µg of RNA using a GoScript reverse transcriptase kit (Promega, Madison, WI, USA) according to the manufacturer's instructions. qPCR was performed using astrocyte cDNA diluted 1:10 and the qPCR SybrGreen Supermix (Qiagen, Valencia, CA, USA) containing forward and reverse primers in RNAse-free water. All reactions were performed in a CFX384 Touch real-time PCR detection system (Biorad, Hercules, CA, USA) and cycling conditions were set as follows: 50°C for 2min; 95°C for 10min; (95°C for 15s; 60°C for 1min) x 40 cycles. To evaluate primer specificity, a melting curve analysis was performed by heating samples from 65°C to 99°C (1°C increment changes at 5s intervals). All sample measurements were performed in duplicate. Primers were designed with PrimerBlast and used at a concentration of 200nM. Data were normalized to the expression of 18S (Fwd 5' CCCAACTTCTTAGAGGGACAAG 3'; Rev 5' CATCTAAGGGCATCACAGACC 3') and the relative quantification value of each target gene was determined using a comparative CT method (31). For virus detection, SARS-CoV-2 nucleocapsid N1 primers were used as previously described (Fwd 5' CAATGCTGCAATCGTGCTAC 3'; Rev 5' GTTGCGACTACGTGATGAGG 3') (32, 33). A serial dilution of SARS-CoV-2 were used as a standard curve. Data were expressed as mean ± SEM. Statistical significance was calculated by a two-tailed unpaired Student's t-test. All analyses were performed using GraphPad Prism 8.0 (San Diego, CA, USA) and a significance level of $p \leq 0.05$ was adopted.

### *Astrocyte bioenergetics*

Astrocytes were plated on Seahorse XF-24 plates at a density of $1.5x10^4$ cells per well and incubated in complete culture medium for two days at 37°C in 5% $CO_2$. 24 hours before the experiment, cells were either infected by SARS-CoV-2 (MOI 0.1) or not infected (MOCK). One day post-infection, the culture medium was changed to Seahorse Base medium (supplemented with 1mM pyruvate, 2mM glutamine and 10mM glucose) and cells were incubated at 37°C in a non-CO2 incubator for 1h. OCR (Oxygen Consumption Rate) was measured over the course of the experiment under basal conditions and after injections of oligomycin (1µM), FCCP (5µM) and antimycin A/rotenone (100nM/1µM). Protein concentration was determined for each well to normalize the data. Data were expressed as mean ± SEM of two independent experiments performed in quintuplicate. Statistical significance was calculated by two-tailed unpaired Student's t-test. All analyses were performed using GraphPad Prism 8.0 software (San Diego, CA, USA) and a significance level of $p \leq 0.05$ was adopted.

### *Differentiation of the SH-SY5Y human neuroblastoma cell line*

The SH-SY5Y cell line (SH-SY5Y-ATCC-CRL-2266) was cultivated using a commonly used neuronal differentiation protocol (34–36) using DMEM/F12 medium, 10% FBS and 1% penicillin-streptomycin at 37°C in humidified air with 5% $CO_2$. The SH-SY5Y cells were plated and, upon reaching 25-30% confluency, the medium was changed to neuronal differentiation medium consisting of DMEM/F12 with 1% FBS and 10µM retinoic acid (Sigma Aldrich). The differentiation medium was replaced every 2-3 days during 2 weeks. These differentiated SH-SY5Y cells are more closely related to adrenergic

neurons, but they also express dopaminergic markers (36). The SH-SY5Y cell line was kindly donated by Prof. Dr. Gustavo J. S. Pereira (Unifesp).

***NSC differentiation into neurons***

The human NSC-derived neurons were cultivated following the protocol described by Thermo Fisher Scientific (37–39). NSCs were plated on geltrex-coated plates and maintained with NEM medium at 37°C in humidified air with 5% $CO_2$. Upon reaching 40% confluency, the medium was changed to neuronal differentiation medium consisting of DMEM/F12 and Neurobasal medium (1:1) with 1% B27 supplement (Thermo Fisher Scientific, Carlsbad, CA, USA) and 1% Glutamax (Thermo Fisher Scientific, Carlsbad, CA, USA). The medium was renewed every four days for 20 days by removing half of the volume and adding the same volume of fresh medium. Medium renewal was performed in this manner since factors secreted by the differentiating cells are important for successful differentiation. Two control cell lines were used: GM23279A, obtained from a female subject (available at Coriell) and BR-1 (14). Both cell lines were cultivated following the protocol described by Thermo Fisher Scientific (16, 40–42).

These cells and protocols have been extensively characterized elsewhere (37–39). We also used FACS analysis for cellular markers and found a bonafide neuronal phenotype due to the expression of the neuronal markers synaptophysin (75.9% of cells), MAP2 (99.9%) and β-tubulin (99%) and astrocytic marker GFAP (8.1%) (Fig. S13).

***CellTiter-Glo luminescent cell viability assay***

Astrocyte and NSC-derived neuron death caused by SARS-CoV-2 infection was measured using ATP quantification by a luminescence assay (Promega, Madison, WI,

USA; G7572). The CellTiter-Glo luminescent cell viability assay determines the number of viable cells in culture through quantitation of ATP levels, which reflect the presence of metabolically active cells. Astrocytes and NSC-derived neurons were infected with SARS-CoV-2 and harvested after 24, 48 or 72h. Astrocytes and NSC-derived neurons were then washed and the CellTiter-Glo reagent was added to the cells, following the manufacturer's instructions (Promega; G7572). The luminescent signals were obtained using a FlexStation 3 (Molecular Devices, CA, USA).

***Calcein AM cell viability assay***

SH-SY5Y death caused by SARS-CoV-2 infection was measured using Calcein AM, a cell-permeant dye that can be used to determine cell viability in most eukaryotic cells. In live cells, the non-fluorescent calcein AM is converted to green, fluorescent calcein, after acetoxymethyl ester hydrolysis by intracellular esterases (Invitrogen, Cat. No. C3100). The SH-SY5Y cell line was infected with SARS-CoV-2 and harvested after 24, 48 or 72h. SH-SY5Y cells were then washed and the approximately 2μM serum-free calcein AM working solution (FluoroBrite™ DMEM, ThermoFisher Scientific) was added to the cells and incubated for 30 minutes at room temperature, according to the manufacturer's protocol. The working solution was removed and replaced with a normal growth medium. The fluorescence signals were obtained using a GloMax® Discover microplate reader (Promega, Madison, WI, USA).

***Exposure of neurons to astrocyte-conditioned media***

Astrocytes, human NSC-derived neurons and SH-SY5Y cells were cultured separately in standard conditions until complete differentiation. First, astrocytes were

infected with SARS-CoV-2 (MOI 0.1 and MOI 1.0) or mock condition (MOCK), and after 24 hours, the medium was removed and cells were washed with PBS and cultured for 24 hours. The media of NSC-derived or SH-SY5Y neurons were removed and replaced by the conditioned media from SARS-CoV-2-infected astrocytes or control medium for 24 hours. After incubation, cells were collected for flow cytometry analysis following the procedure described below, and also for viral load evaluation using RT-PCR. We also evaluated the cell viability of SH-SY5Y cells exposed to astrocyte-conditioned media using CellTiter-Glo luminescent cell viability assay.

***Flow cytometry analyses***

The expression of GFAP, synaptophysin, MAP2 and β-tubulin was evaluated through FACS analysis. Astrocytes and NSC-derived neurons were collected and stained with BD Horizon fixable viability stain 510 for 30min at 4°C. Primary antibodies anti-GFAP (Abcam; Cat. Ab7260); anti-synaptophysin D35E4 (Cell Signaling; Cat.#5461); XP Rabbit mAb (Cell Signaling; Cat. #5461); anti-MAP2 (Abcam; Cat. ab32454); and anti-tubulin, beta III isoform, C-terminus (Milipore; Cat. #MAB1637) all diluted in BD Perm/Wash buffer, were added to the cells and incubated for 1h at 4°C (1:500). Secondary antibodies donkey anti-mouse IgG AlexaFluor 594 (Cell Signalling; Cat. 8890S), donkey anti-rabbit IgG AlexaFluor 647 (Abcam; Cat. ab15006) and donkey anti-goat IgG AlexaFluor 488 (Abcam; Cat. ab150129), all diluted in BD Perm/Wash buffer, were added and incubated for 30min at 4°C (1:250). Cells were washed with BD Perm/Wash buffer and then transferred to polypropylene FACS tubes. Analyses were carried out on a FACSymphony (Becton & Dickinson, San Diego, CA, USA).

The viability of human NSC-derived and SH-SY5Y neurons was determined 24h after incubation with the conditioned medium of SARS-CoV-2-infected astrocytes or control medium. The percentage of live (Apotracker-/FVS510-), necrotic (Apotracker-/FVS510+), early apoptotic (Apotracker+/FVS510-) and late apoptotic (Apotracker+/FVS510+) cells was determined by flow cytometry (FACSymphony, Becton & Dickinson, San Diego, CA, USA), after labeling with fixable viability stain (FVS510, BD Biosciences, #564406) and Apotracker Green (BioLegend, #427403). Data were analyzed using FlowJo software (BD Biosciences). Data are representative of at least two independent experiments performed in triplicate and are shown as mean ± SEM. P values were determined by one-way ANOVA followed by Tukey's post hoc test.

***Data availability***

The mass spectrometry proteomic data have been deposited to the ProteomeXchange Consortium via the PRIDE (43) partner repository with the dataset identifiers PXD023781 and 10.6019/PXD023781.

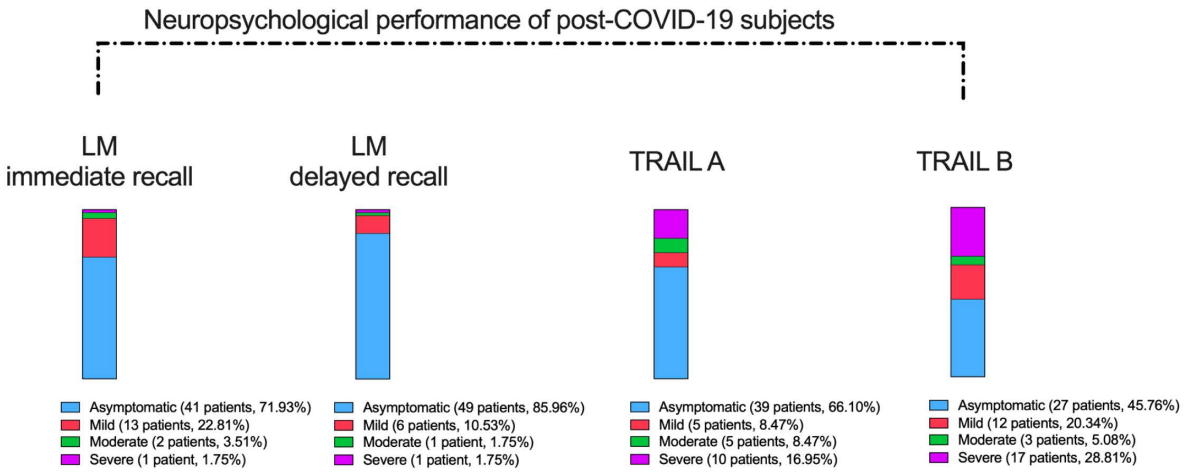


**Fig.S1**. **Frequency of neuropsychological impairment in individuals after mild infection.** The severity of impairments in verbal logical memory (LM; Wechsler Memory Scale-revised) and executive function (Color Trails Tests A and B). The subgroup of individuals who underwent neuropsychological evaluation presented a median age of 35 years (95% CI 33-41 years; range 21-63 years), 16 years of education (95% CI 15-16 years; range 6-24 years), and 59 days after COVID-19 diagnosis (95% CI 46-64 days; range 21-120 days).

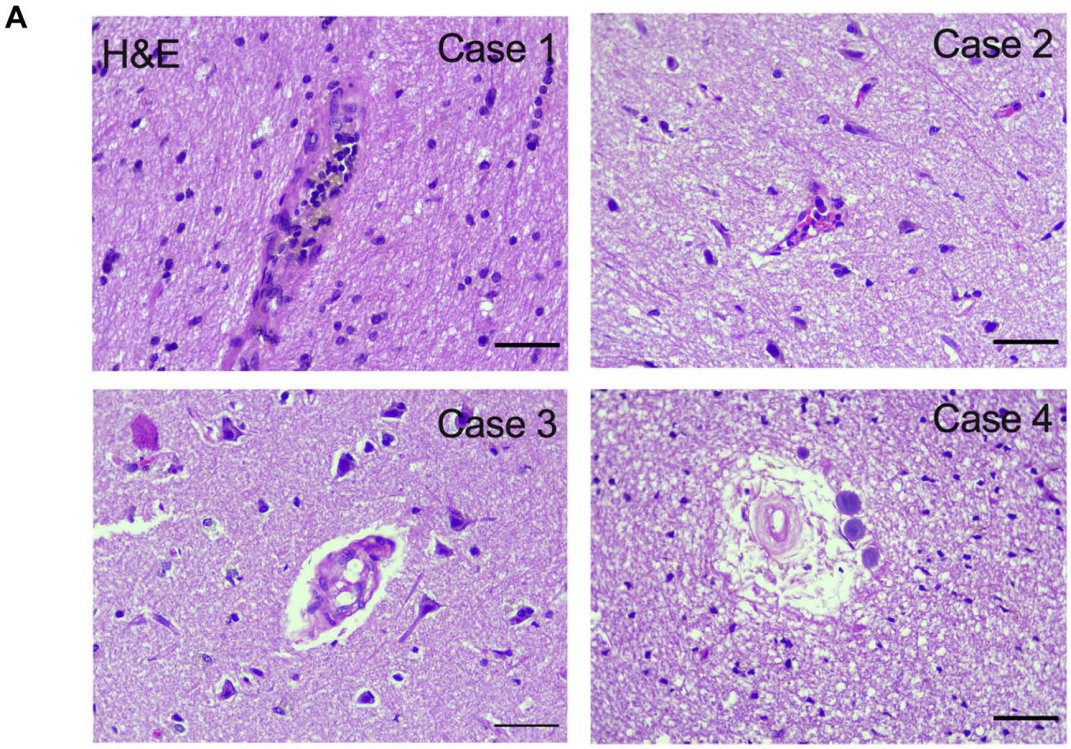
A
H&E
Case 1
Case 2
Case 3
Case 4

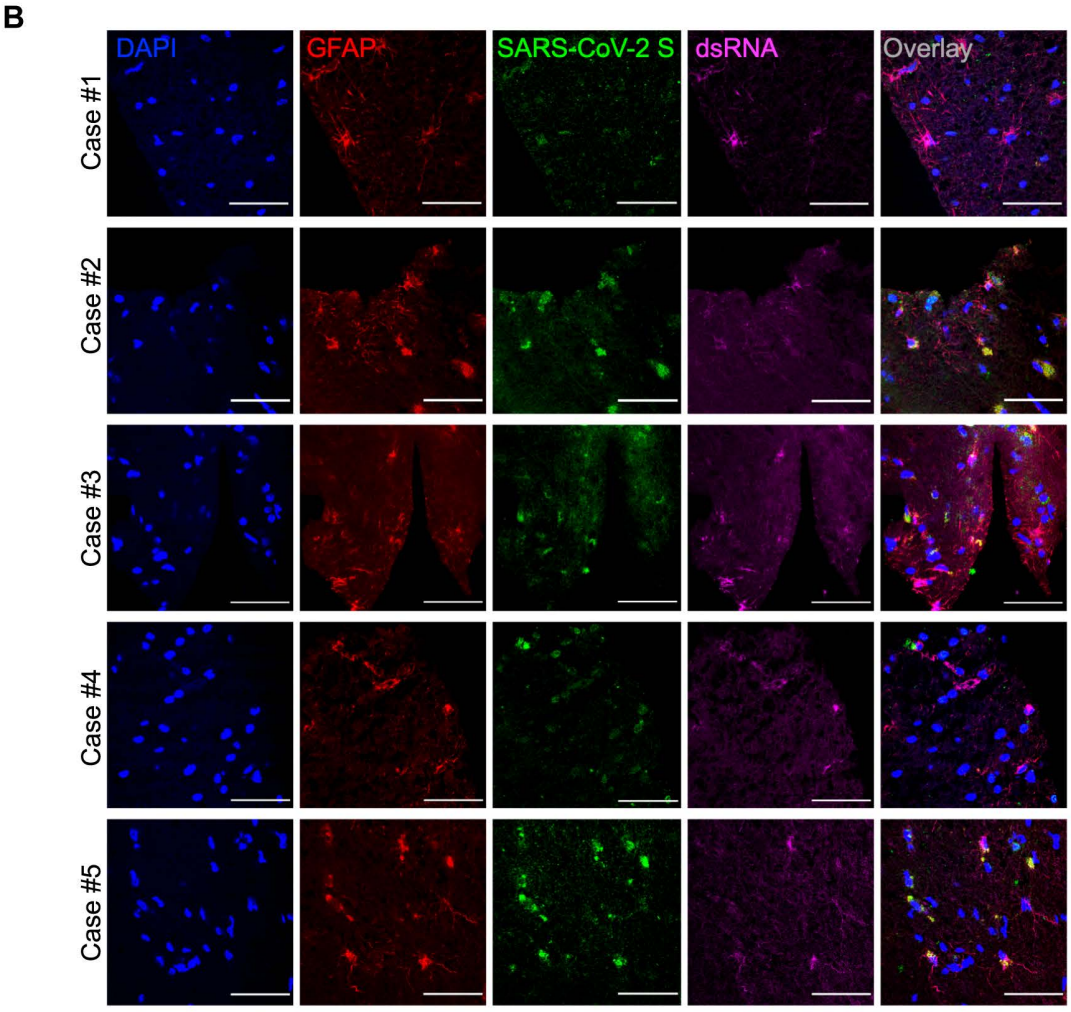
B
DAPI
GFAP
SARS-CoV-2 S
dsRNA
Overlay
Case #1
Case #2
Case #3
Case #4
Case #5

**Fig.S2. SARS-CoV-2 infects the central nervous system and replicates in astrocytes.** (A) Histopathological alterations revealed by H&E images of *postmortem* brain tissue from individuals who died of COVID-19. Samples from 26 individuals were analyzed; 5 showed alterations. Case 1: intraparenchymal cerebral vessel with margination of inflammatory cells through endothelium; Case 2: focal infiltration of inflammatory cells – diapedesis; Case 3: intraparenchymal vascular damage; Case 4: perivascular edema and senile corpora amylacea. Case 5 is also shown in Figure 2. (B) Representative confocal images of the brain tissue of the 5 COVID-19 patients who manifested histopathological alterations. Staining of glial fibrillary acidic protein (GFAP, red), double-stranded RNA (dsRNA, magenta), SARS-CoV-2-S (green) and nuclei (DAPI, blue). Images were acquired with 630x magnification. Scale bar indicates 50μm.

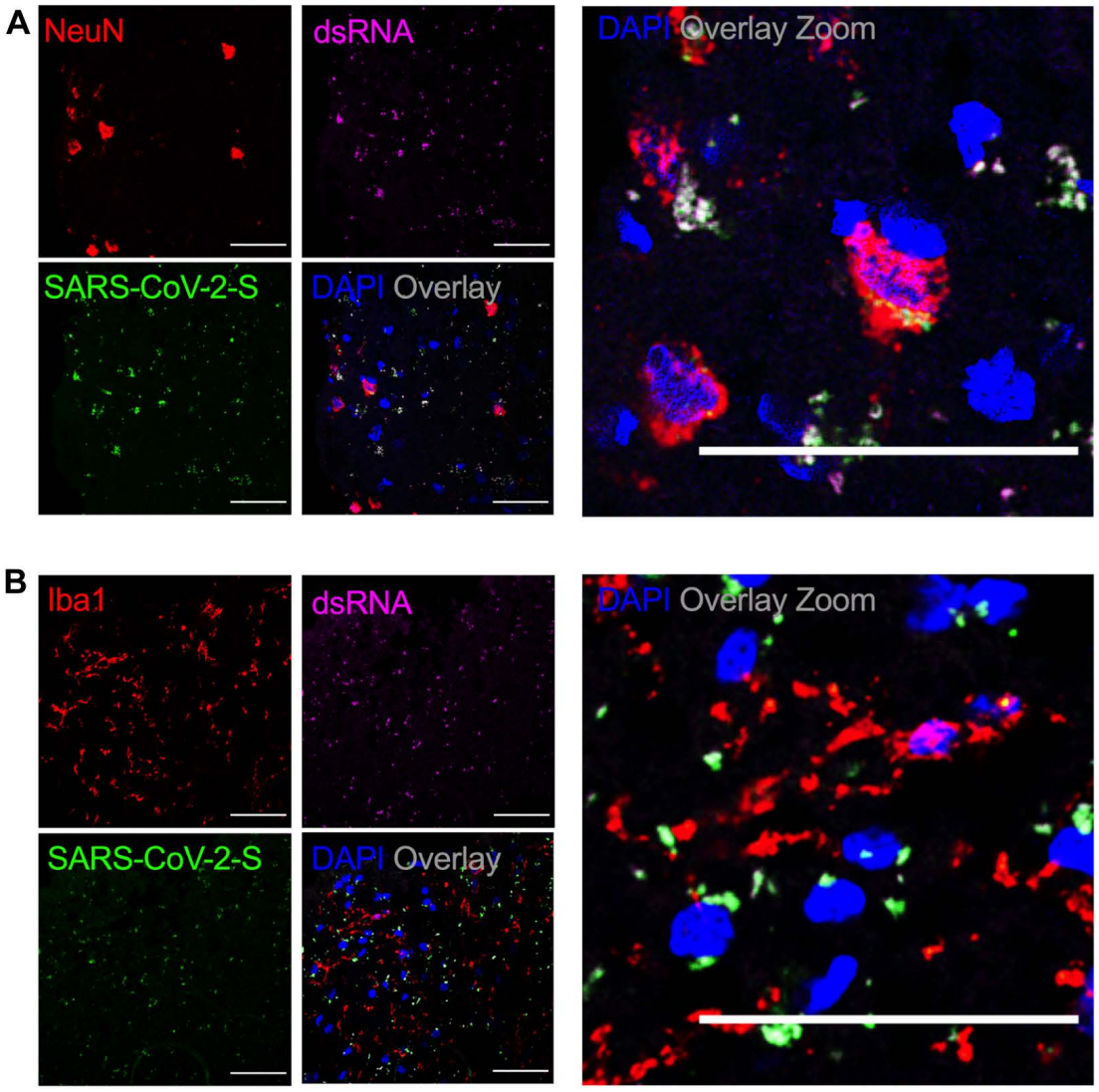
A
NeuN
dsRNA
SARS-CoV-2-S
DAPI Overlay
DAPI Overlay Zoom
B
Iba1
dsRNA
SARS-CoV-2-S
DAPI Overlay
DAPI Overlay Zoom
C
r= 0.5748 p<0.0001
GFAP:dsRNA (correlation coefficient)
GFAP:SARS-CoV-2-S1 (correlation coefficient)
0.0
0.2
0.4
0.6
0.8
D
0.0047
<0.0001
<0.0001
% cells/field
0
20
40
60
80
100
Iba-1+
NeuN+
GFAP+

**Fig.S3. SARS-CoV-2 infects neurons, but not microglia, in the brains of COVID-19 patients.** (A-B) Representative immunostaining and confocal analysis from brain slices from autopsies of COVID-19 patients (n=5). The image depicts staining for: (B) nuclei (DAPI, blue), NeuN (red, neuronal marker), dsRNA (magenta) and SARS-CoV-2-S (green); and (C) nuclei (DAPI, blue), ionized calcium-binding adaptor molecule 1 (Iba1, red, microglial marker), dsRNA (magenta) and SARS-CoV-2-S (green). Images were acquired with 630x magnification. Scale bar indicates 50μm. (C) Pearson's correlation coefficient demonstrating colocalization of SARS-CoV-2-S and dsRNA within GFAP-positive cells. (D) Quantification of CNS cells in the human brain. Percentage of Iba-1-, NeuN- or GFAP-positive cells in the tissues from the five fatal cases of COVID-19. The data are shown as mean ± SEM. P-values were determined by one-way ANOVA followed by Tukey's post-hoc test.

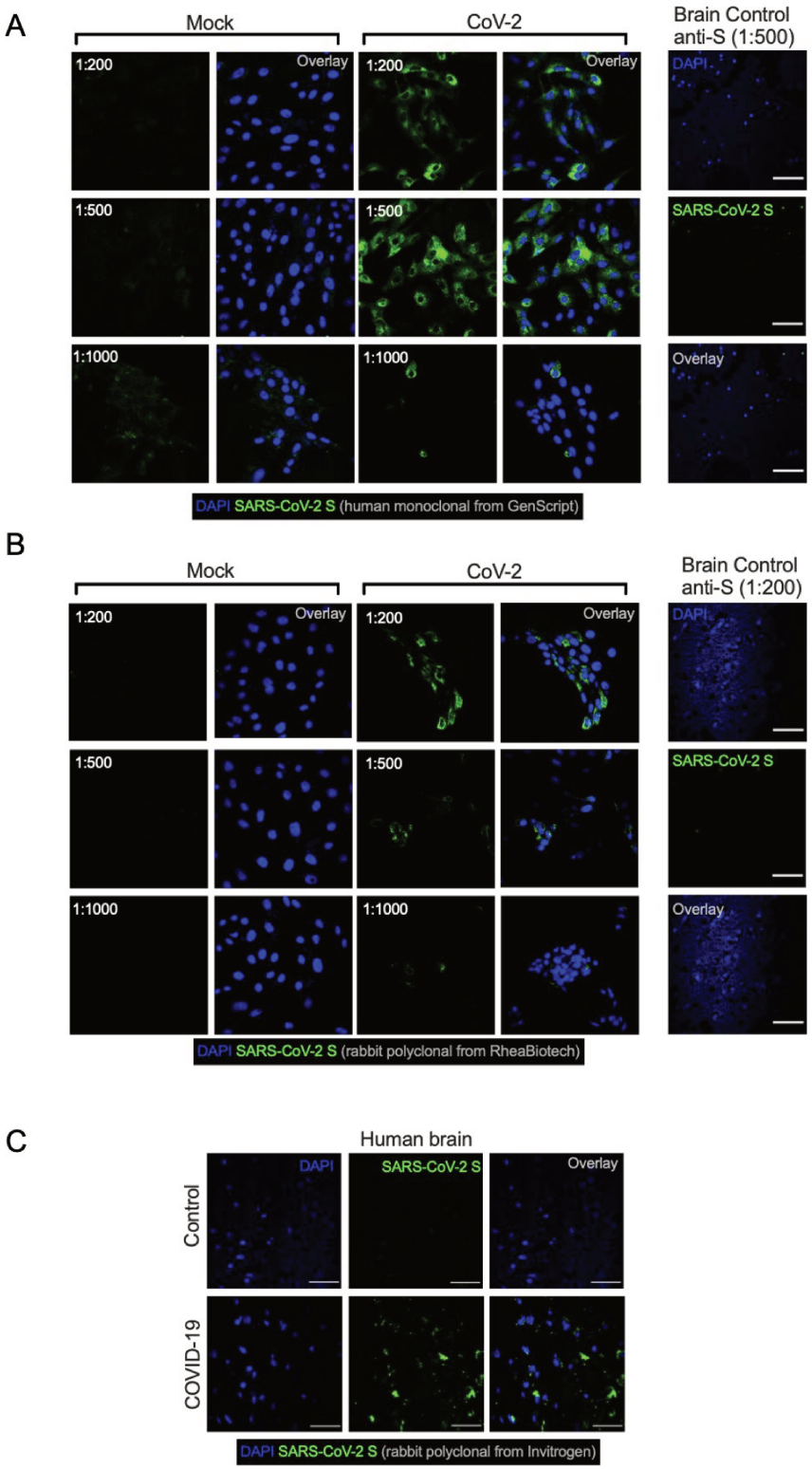
A
Mock
CoV-2
Brain Control
anti-S (1:500)
1:200
Overlay
1:200
Overlay
DAPI
1:500
1:500
SARS-CoV-2 S
1:1000
1:1000
Overlay
DAPI SARS-CoV-2 S (human monoclonal from GenScript)
B
Mock
CoV-2
Brain Control
anti-S (1:200)
1:200
Overlay
1:200
Overlay
DAPI
1:500
1:500
SARS-CoV-2 S
1:1000
1:1000
Overlay
DAPI SARS-CoV-2 S (rabbit polyclonal from RheaBiotech)
C
Human brain
DAPI
SARS-CoV-2 S
Overlay
Control
COVID-19
DAPI SARS-CoV-2 S (rabbit polyclonal from Invitrogen)

**Fig.S4. Validation of antibodies against SARS-CoV-2 spike (S) protein.** Representative immunostaining and confocal analysis in SARS-CoV-2-infected Vero cells and brain slices from control cases (non-COVID-19) staining with different titrations for anti-S antibodies (1:200, 1:500 and 1:1000). Immunofluorescence images show: nuclei (DAPI, blue) and (A) SARS-CoV-2-S (green, human chimeric monoclonal anti-SARS-CoV-2 spike S1, GeneScript, clone HC2001, Cat. A02038), (B) SARS-CoV-2-S (green, rabbit polyclonal anti-SARS-CoV-2 spike, Rhea Biotech, Cat. IM-0828) or (C) SARS-CoV-2-S (green, rabbit monoclonal anti-SARS-CoV-2 spike, clone T01KHuRb, Cat. 703959). Images were acquired with 630x magnification at the same laser intensity. Scale bar indicates 50µm.

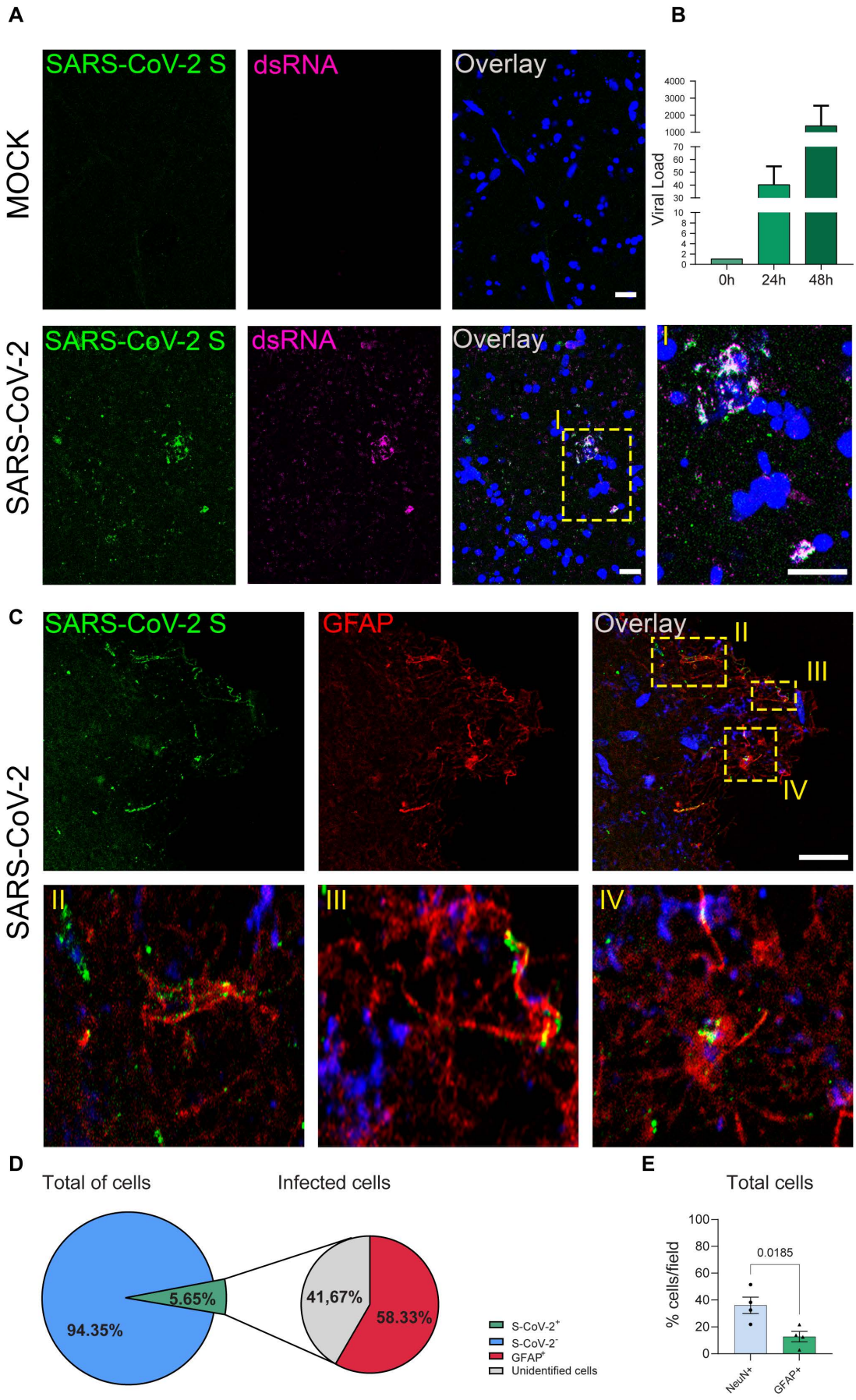
A
B
MOCK
SARS-CoV-2
SARS-CoV-2 S
dsRNA
Overlay
Viral Load
4000
3000
2000
1000
70
60
50
40
30
10
8
6
4
2
0
0h
24h
48h
I
C
GFAP
II
III
IV
D
Total of cells
Infected cells
5.65%
94.35%
41,67%
58.33%
S-CoV-2+
S-CoV-2-
GFAP+
Unidentified cells
E
Total cells
% cells/field
100
80
60
40
20
0
0.0185
NeuN+
GFAP+

**Fig. S5. SARS-CoV-2 infects, replicates in, and preferentially targets astrocytes in adult human brain slices**. (A) Representative images of uninfected control (mock) and SARS-CoV-2-infected human brain slices. Tissue sections were stained for SARS-CoV-2 spike protein (green), double stranded RNA (magenta), and nuclei (DAPI, blue), as indicated. Scale bar indicates 20 μm. Higher magnification is shown in I. (B) Viral load determined by RT-PCR in a human brain slice infected by SARS-CoV-2 at 0, 24, and 48 hpi compared to mock slices (n=2 slices from one patient). (C) Representative cells double-labeled with SARS-CoV-2 spike protein (green) and GFAP (red) are shown at a higher magnification in II, III, and IV. Scale bar indicates 20 μm. (D) Quantification of cells positive for SARS-CoV-2 spike protein and GFAP in human brain slices (n=2 fields from one patient). (E) Quantification of CNS cells in SARS-CoV-2-infected brain slices. Percentage of NeuN- or GFAP-positive cells. The data are shown as mean ± SEM. P-values were determined by a two-tailed unpaired Student t-test.

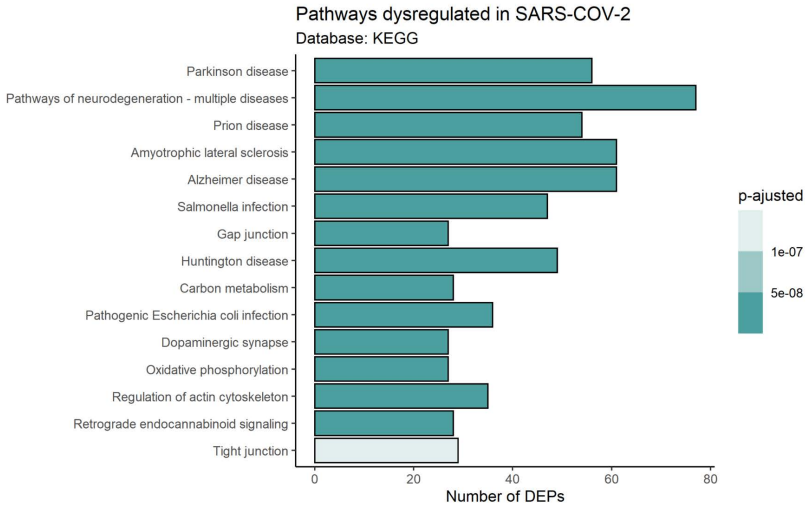


**Fig.S6. Proteomic analysis of *postmortem* brain tissue from patients who died with COVID-19.** Top 15 enriched pathways by differentially expressed proteins in *postmortem* brain tissue from patients who died with COVID-19 (as per KEGG database). Dot color represents lower (blue) or higher (red) expression or no change (gray). Bar color represents the p value adjusted by the false discovery rate (FDR).

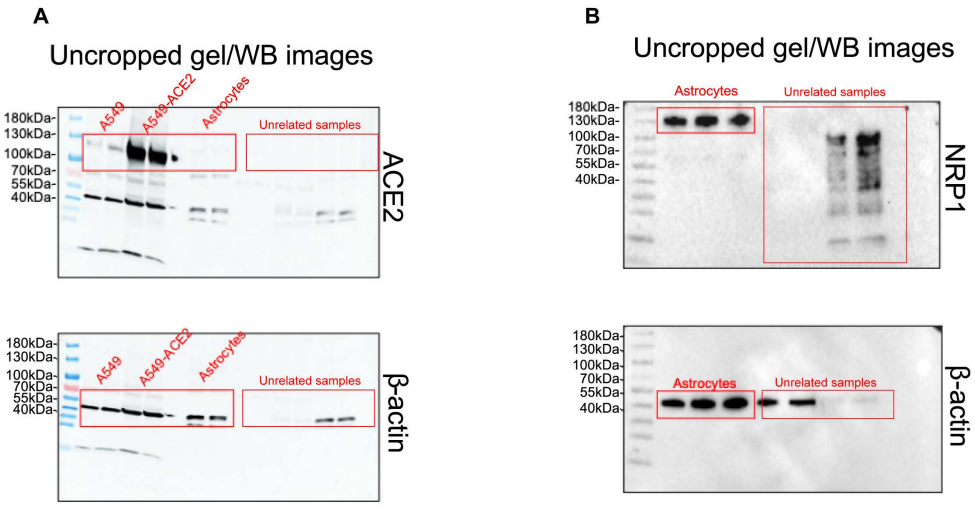


**Fig.S7. Full scan of the original uncropped immunoblots.** (A) Original immunoblots used in Figure 5C for (A) ACE2 and β-actin, and (B) for NRP1 and β-actin. Regions of interest were cropped as indicated in red lines.

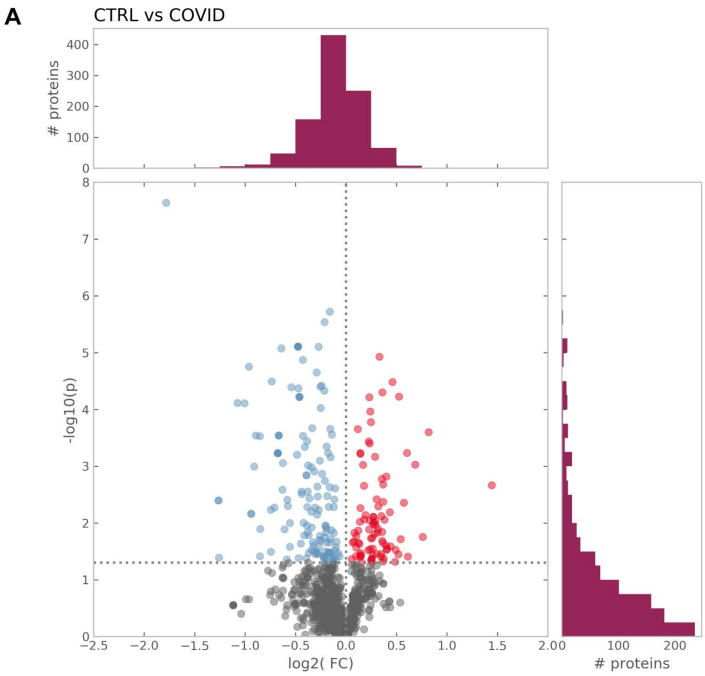
A
CTRL vs COVID
# proteins
-log10(p)
log2( FC)
# proteins

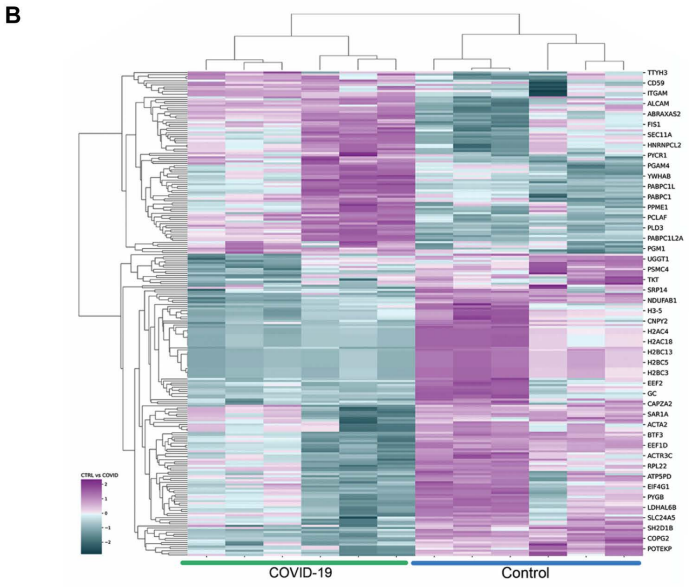
B
TTYH3
CD59
ITGAM
ALCAM
ABRAXAS2
FIS1
SEC11A
HNRNPCL2
PYCR1
PGAM4
YWHAB
PABPC1L
PABPC1
PPME1
PCLAF
PLD3
PABPC1L2A
PGM1
UGGT1
PSMC4
TKT
SRP14
NDUFAB1
H3-5
CNPY2
H2AC4
H2AC18
H2BC13
H2BC5
H2BC3
EEF2
GC
CAPZA2
SAR1A
ACTA2
BTF3
EEF1D
ACTR3C
RPL22
ATP5PD
EIF4G1
PYGB
LDHAL6B
SLC24A5
SH2D1B
COPG2
POTEKP
CTRL vs COVID
COVID-19
Control

**Fig.S8. Proteomic analysis of SARS-CoV-2-infected astrocytes and *postmortem* brain tissue from patients who died with COVID-19.** (A) Volcano plot representing all the differentially expressed proteins found in astrocytes after SARS-CoV-2 infection. Dot color represents lower (blue) or higher (red) expression or no change (gray). (B) Hierarchical clustering of differentially expressed proteins in human neural stem cell-derived astrocytes that were infected *in vitro* with SARS-CoV-2 (MOI 0.1) for 1h, washed thoroughly, and harvested after 24h. Mock infection was used as a control.

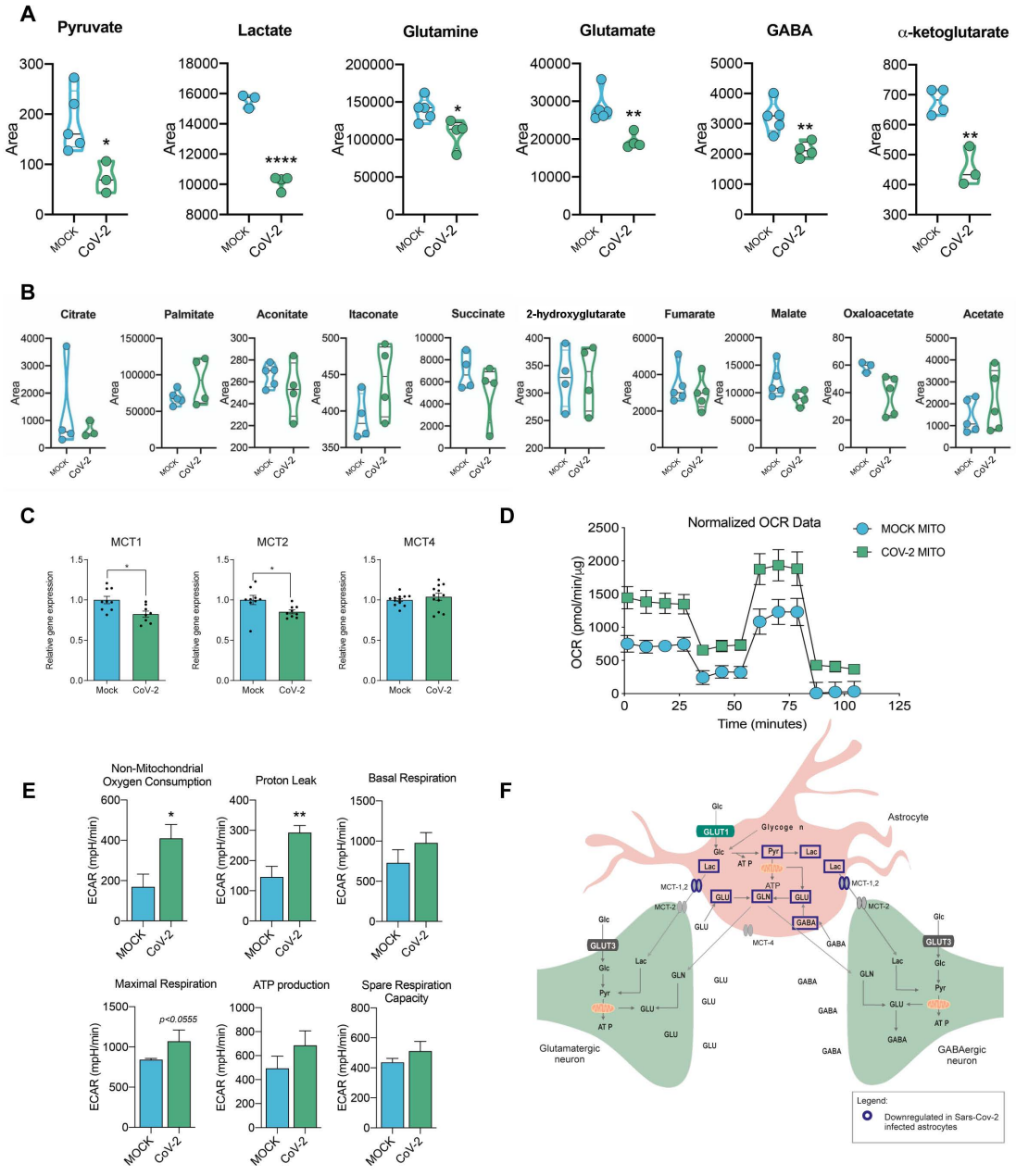


**Fig.S9. Metabolomic analysis of SARS-CoV-2-infected astrocytes.** Human neural stem cell-derived astrocytes were infected in vitro with SARS-CoV-2 (MOI 0.1) for 1h, washed thoroughly and harvested after 24h. Mock infection was used as a control. (A) High-resolution mass spectrometry-based quantification of pyruvate, lactate, glutamine, glutamate, GABA and α-ketoglutarate in SARS-CoV-2 infected astrocytes vs. mock. (B)

High-resolution mass spectrometry quantification of citrate, palmitate, aconitate, itaconate, succinate, 2-hydroxyglutarate, fumarate, malate, oxaloacetate and acetate in SARS-CoV-2 infected astrocytes vs. mock. The integration area of each peak was used to calculate the violin plot graph and an unpaired t-test with Welch's correction was used for statistical comparison. (C) Relative gene expression of *MCT1*, *MCT2*, and *MCT4* in astrocytes after SARS-CoV-2 infection. These data were obtained by RT-qPCR and normalized to the expression of the *ACTB* gene. Relative quantification of each target gene was analyzed using a comparative CT method. (D-E) Oxygen consumption rate (OCR) of SARS-CoV-2 infected astrocytes vs. mock. SeaHorse Flux Analysis using the MitoStress test where basal respiration was measured followed by determination of respiration in response to oligomycin, FCCP and rotenone/antimycin. Data are representative of at least two independent experiments performed in triplicate (metabolomics or RT-qPCR) or quintuplicate (SeaHorse Flux analysis), and shown as mean ± SEM. P-values were determined by two-tailed unpaired t-test with Welch's correction. *$P < 0.05$; **$P < 0.01$; **** $P < 0.0001$ compared to mock. (F) Diagram summarizing the changes in metabolite levels and *MCTs* alterations in SARS-CoV-2-infected astrocytes.

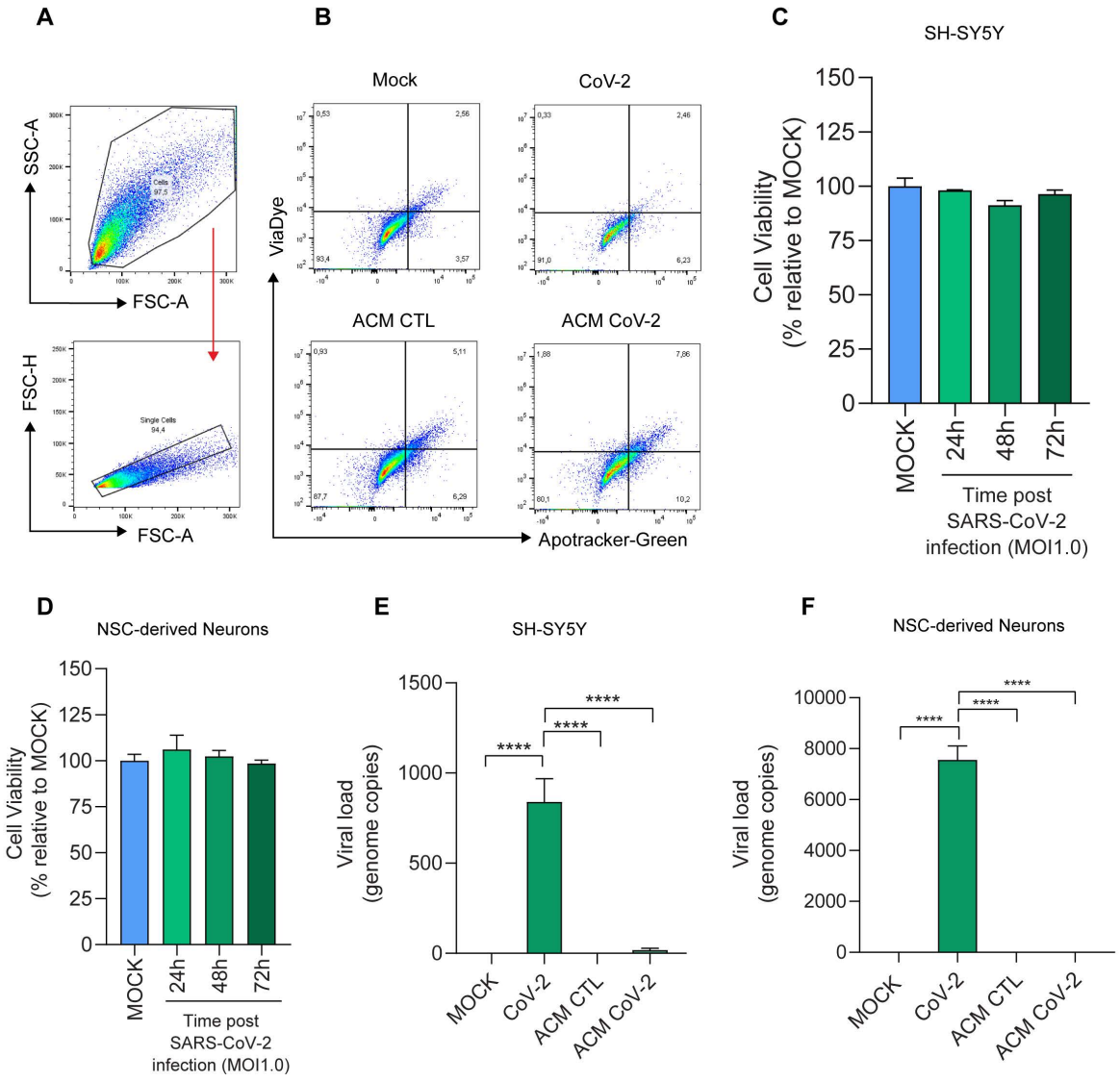


**Fig.S10. Medium conditioned by SARS-CoV-2-infected astrocytes reduces neuronal viability despite no change from direct virus exposure to neurons.** Differentiated SH-SY5Y cells were cultured for 24h in the presence of medium conditioned by SARS-CoV-2-infected astrocytes (ACM CoV-2) or uninfected astrocytes (ACM CTL). Cellular viability was measured by apotracker/fixable viability stain (FVS) and analyzed by flow cytometry. (A) Representative gating strategies. (B) Representative dot-plots of neuronal

viability. (C) SH-SY5Y neuronal and (D) NSC-derived neuron cell viability upon SARS-CoV-2 infection. The cells were infected *in vitro* with SARS-CoV-2 (MOI 1.0) for 1h, washed thoroughly and harvested after 24h. Mock infection was used as a control. SH-SY5Y viability was assessed using calcein AM staining (Invitrogen) at 24, 48 and 72 hours post-infection. The NSC-derived neurons were assessed using an ATP-quantifying, luminescence-based cell viability assay (CellTiter-Glo) at 24h, 48h and 72h post-infection. (E) SARS-CoV-2 viral load detection in differentiated SH-SY5Y neurons and in (F) NSC-derived neurons using RT-PCR after 24h in the presence of mock, SARS-CoV-2 (MOI 1.0) or medium conditioned by either SARS-CoV-2-infected astrocytes (ACM CoV-2) or uninfected astrocytes (ACM CTL). Data are representative of two independent experiments performed in triplicate, and shown as mean ± SEM. P-values were determined by one-way ANOVA followed by Tukey's post hoc test. ***$P < 0.001$; ****$P < 0.0001$ compared to the mock group.

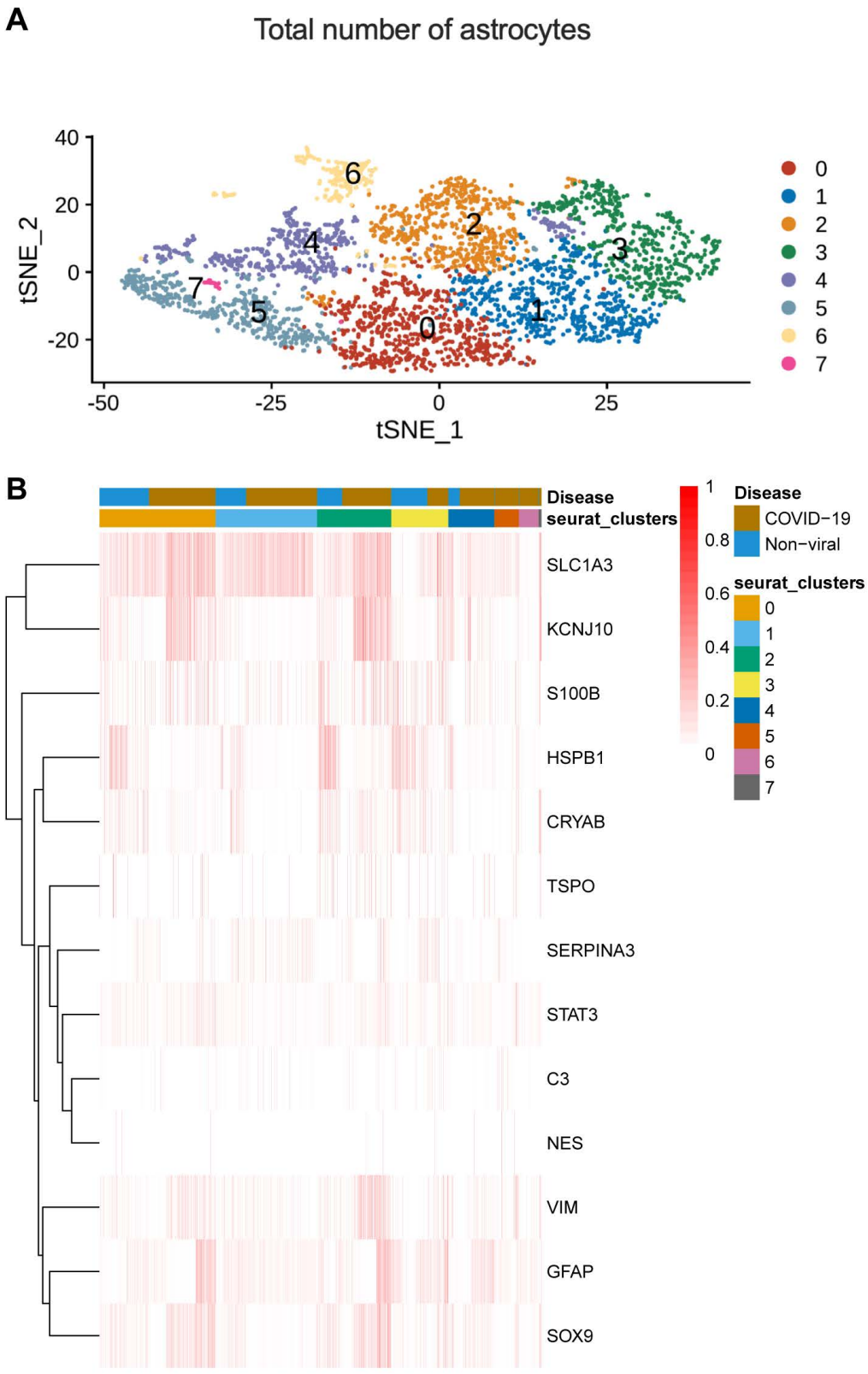
A
Total number of astrocytes
tSNE_2
tSNE_1
40
20
0
-20
-50
-25
0
25
0
1
2
3
4
5
6
7
B
Disease
seurat_clusters
SLC1A3
KCNJ10
S100B
HSPB1
CRYAB
TSPO
SERPINA3
STAT3
C3
NES
VIM
GFAP
SOX9
1
0.8
0.6
0.4
0.2
0
Disease
COVID−19
Non−viral
seurat_clusters
0
1
2
3
4
5
6
7

**Fig.S11.** Reactive astrogliosis markers were enriched in the brains of COVID-19 patients. (A) Representative tSNE plot of total astrocytes, and (B) Seurat tSNE Heatmap of expression of reactive astrogliosis markers by single nucleus RNAseq analysis from the infected controls and patients with COVID-19. Data analysis revealed the presence of 8 different clusters, and reactive astrogliosis markers were enriched in samples from COVID-19 compared to non-infected controls.

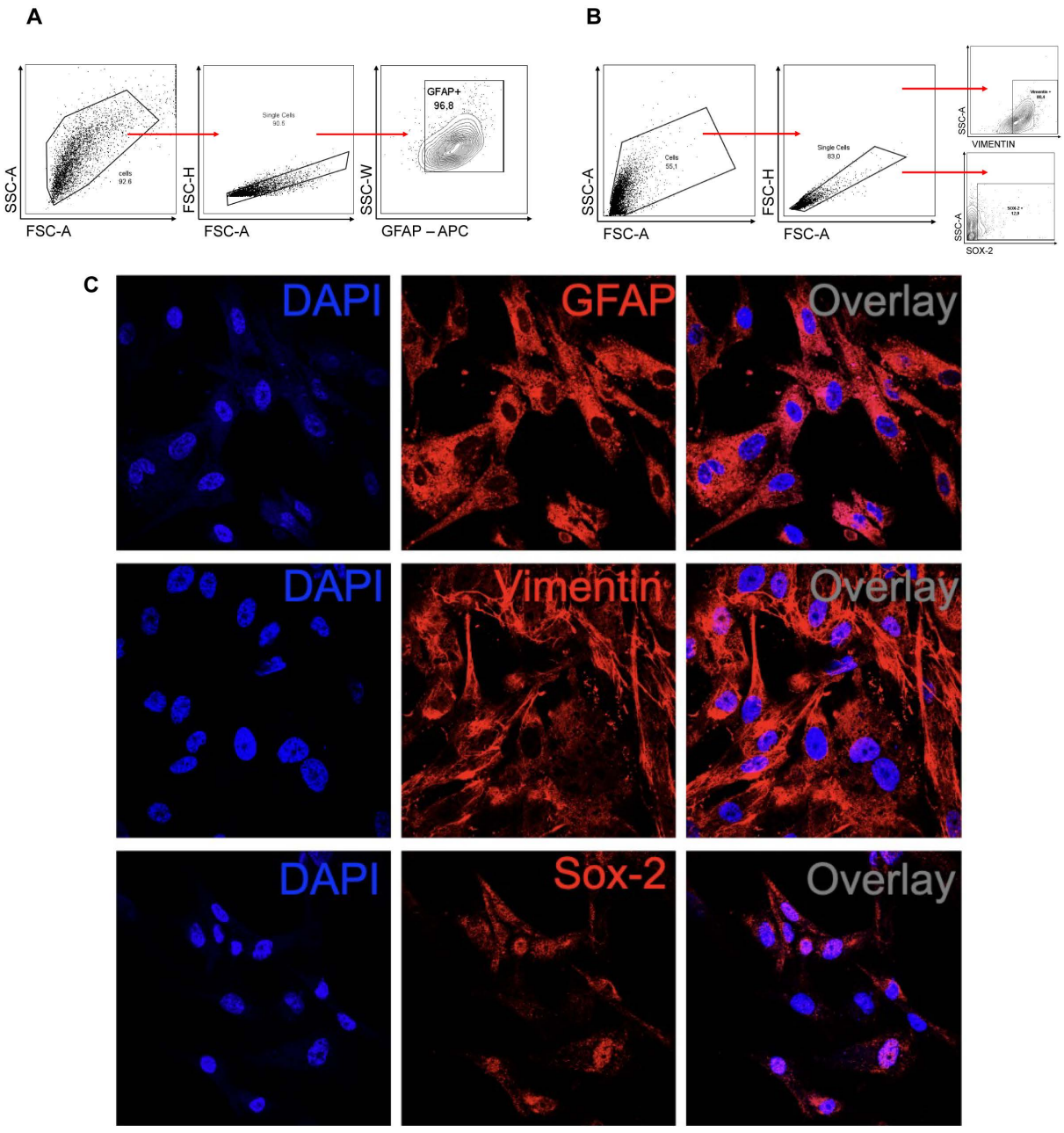


**Fig.S12. Characterization of human astrocyte cultures.** Cells were trypsinized for FACS analysis and incubated with antibodies against GFAP, vimentin and SOX-2. (A) Cells were analyzed and the results were plotted as SSC-A *vs.* GFAP (APC). The percentage of positive cells is indicated in the representative contour plot. (B) Cells were

analyzed and the results were plotted as SSC-A *vs.* SOX-2 (APC) and SSC-A *vs.* vimentin (BB515). The percentage of positive cells is indicated in the representative contour plot. (C) Staining for GFAP, vimentin, SOX-2 (red) and nuclei (DAPI, blue). Images were acquired with 630x magnification. Scale bar indicates 50µm.

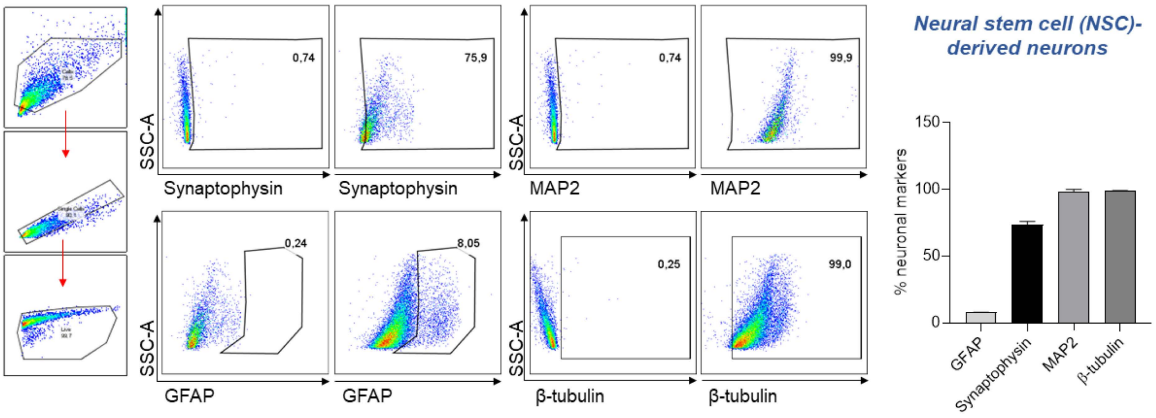


**Fig.S13. Characterization of human neural stem cell-derived neurons**. The cells were trypsinized for FACS analysis and incubated with antibodies against synaptophysin, MAP2, GFAP and β-tubulin. Cells were analyzed and the results were plotted as SSC-A *vs.* synaptophysin, MAP2, GFAP or β-tubulin. The percentage of positive cells is indicated in the representative contour plot.

**Table S1:** Epidemiological and Clinical data from patients and controls included in the *in vivo* analyses.

| **Demographics** | **COVID-19** | **Healthy Volunteers** | **p-value** |
|---|---|---|---|
| Number | 81 | 81 | |
| Age median (range) | 36 years (21-71) | 36 years (21-68) | 0.97 |
| Sex (women/men) | 61/20 | 54/27 | 0.3 |
| Education median (range) | 16 years (6-24) | 17 years (8-25) | <0.01 |
| 95% CI [lower-upper limits] | [14-16] | [17-18] | |
| **Comorbidities** | | | |
| Diabetes | 1 | 3 | 0.6 |
| Asthma | 3 | 2 | 1 |
| Hypertension | 11 | 6 | 0.3 |
| Dyslipidemia | 1 | 5 | 0.2 |
| Past history of neuropsychiatric diagnosis | 1 depression; 3 anxiety; 2 anxiety+ depression; 1 schizophrenia | none | -- |
| **Present symptons** | | | |
| BAI median (range) | 5(0-35) | 1(0-10) | <0.001 |
| 95% CI [lower - upper limits] | 69 responses [2-8] | 81 responses [1-3] | |
| BDI-II median (range) | 6 (0-45) | 3 (0-12) | <0.001 |
| 95% CI [lower - upper limits] | 69 responses [4-8] | 81 responses [2-4] | |
| CFQ median (range) | 16 (0-32) | 5 (0-22) | <0.001 |
| 95% CI [lower - upper limits] | 62 responses [11-18] | 78 responses [3-8] | |
| ESS median (range) | 8.5 (0-19) | 6 (0-12) | 0.003 |
| 95% CI [lower - upper limits] | 62 responses [7-10] | 78 responses [5-7] | |

* The levels of anxiety, depression, fatigue and sleepiness were higher for patients. Groups were balanced for age and sex. COVID-19: *Coronavirus Disease 19*; HV: *Healthy Volunteers*; DM: *Diabetes Mellitus*; BAI: *Beck Anxiety Inventory*; BDI-II: *Beck Depression Inventory*; CFQ: *Chalder Fatigue Questionnaire*; ESS: *Epworth Sleepiness Scale*; CI: *Confidence Interval*. MRI acquisition periods: COVID-19 Patients (July-September 2020); Healthy volunteers (July 2020- December 2021)

**Table S2:** Results from neuropsychological tests (in z-scores) from post-COVID individuals. Results were adjusted for sex, age and education.

| | Median | 95% CI [lower; upper limits] | Range |
|---|---|---|---|
| **Logical memory (immediate recall)** | -0.630 | [-0.921; -0.339] | -2.25 to 1.96 |
| **Logical memory (delayed recall)** | -0.270 | [-0.540; 0.00] | -2.37 to 1.58 |
| **Color Trail A** | -0.70 | [-0.540; 0.00] | -7.05 to 0.77 |
| **Color Trail B** | -1.13 | [-1.559; -0.70] | -5.55 to 1.25 |

* CI: *Confidence Interval*.

**Table S3:** Partial correlations between neuropsychological scores and cortical thickness (fatigue scores were used as covariate).

| | Correlation coefficient | CI 95% [lower; upper limits] | Significance | FDR adjusted significance |
|---|---|---|---|---|
| **BAI x left gyrus rectus** | 0.053 | [-0.235; 0.332] | 0.72 | 0.720 |
| **BAI x right gyrus rectus** | -0.356 | [-0.581; -0.080] | 0.013 | 0.026 |
| **BAI x left gyrus orbital** | -0.186 | [-0.446; 0.014] | 0.206 | 0.274 |
| **BAI x right gyrus orbital** | -0.401 | [-0.615; -0.132] | 0.005 | 0.019 |
| | | | | |
| **Immediate logical memory x left IFG (pars opercularis)** | 0.357 | [0.070; 0.589] | 0.016 | 0.023 |
| **Immediate logical memory x right IFG (pars opercularis)** | 0.303 | [0.011; 0.548] | 0.043 | 0.043 |
| **Immediate logical memory x left IFG (pars triangularis)** | 0.420 | [0.144; 0.635] | 0.004 | 0.008 |
| **Immediate logical memory x right IFG (pars triangularis)** | 0.487 | [0.226; 0.683] | 0.001 | 0.004 |
| **Immediate logical memory x left STG (planum temporale)** | 0.425 | [0.150; 0.639] | 0.004 | 0.008 |
| **Immediate logical memory x right STG (planum temporale)** | 0.349 | [0.061; 0.582] | 0.019 | 0.023 |
| | | | | |
| **Color Trail B x Left gyrus rectus** | 0.226 | [-0.066; 0.482] | 0.127 | 0.166 |
| **Color Trail B x Right gyrus rectus** | 0.205 | [-0.087; 0.465] | 0.166 | 0.166 |

COVID-19: *Coronavirus Disease 19*; BAI: *Beck Anxiety Inventory*; IFG: *Inferior Frontal Gyrus*; STG: *Superior Temporal Gyrus*; CI: *Confidence Interval*; FDR: *False Discovery Rate*.

**Table S4** : COVID-19 patient characteristics

| **Demographics** | | **%** |
|---|---|---|
| Number | 26 | |
| Age (years) | 66.08±14.89 | |
| Hospital day | 12.8±10.08 | |
| Female | 10 | 38.46% |
| **Comorbities** | | |
| Hypertension | 20 | 76.92% |
| Diabetes | 13 | 50% |
| Obesity | 12 | 46% |
| Lung disease | 2 | 7.69% |
| History of smoking | 8 | 30.76% |
| Heart disease | 10 | 38.46% |
| Kidney disease | 5 | 19.23% |
| Cerebrovascular accident | 4 | 15.38% |
| Cancer | 2 | 7.69% |
| Autoimmune diseases | 3 | 11.53% |
| Immune deficiency | 2 | 7.69% |
| **Laboratory findings** | | |
| CRP (mg/dL)* | 13.81±7.125 | |
| D-Dimers (µg/mL)** | 3.84±2.94 | |
| LDH (U/L)# | 631.6±481.2 | |
| Ferritin (ng/mL)& | 1,566±1,381 | |
| Haemoglobin (g/dL) | 11.73±2.33 | |
| Neutrophils (cell/$mm^3$) | 7,632±4,474 | |
| Lymphocytes (cell/$mm^3$) | 2,955±9,053 | |
| Platelets (count/$mm^3$) | 201,682±122,865 | |
| **Medications** | | |
| Antibiotics | 25 | 96.1% |
| Heparin | 25 | 96.1% |
| Antimalarial | 1 | 3.84% |
| Oseltamivir | 15 | 57.69% |
| Glucocorticoids | 11 | 42.30% |
| **Respiratory status** | | |
| Mechanical ventilation | 26 | 100% |
| Nasal-cannula oxygen | 22 | 84.61% |
| $pO_2$ | 74.45±18.13 | |
| $SatO_2$ | 91.80±7.859 | |
| **Outcome** | | |
| Deaths | 26 | 100% |

**CRP: C-reactive protein (Normal value <0.5 mg/dL);*
***D-dimers (NV <0.5 µg/mL); #LDH: lactic dehydrogenase (Normal range: 120-246 U/L); &Ferritin (NR: 10-291 ng/mL).*

**Table S5:** Clinical data of five COVID-19 patients who manifested histopathological alterations in the brain

| **Demographics** | | **%** |
|---|---|---|
| Number | 5 | |
| Age (years) | 73.0±14.02 | |
| Hospital day | 7.0±3.317 | |
| Female | 1 | 20% |
| **Comorbities** | | |
| Hypertension | 5 | 100% |
| Diabetes | 3 | 60% |
| Obesity | 1 | 20% |
| Lung disease | 0 | 0% |
| History of smoking | 3 | 60% |
| Heart disease | 2 | 40% |
| Kidney disease | 1 | 20% |
| Cerebrovascular accident | 0 | 0% |
| Cancer | 0 | 0% |
| Autoimmune diseases | 0 | 0% |
| Immune deficiency | 0 | 0% |
| **Laboratory findings** | | |
| CRP (mg/dL)* | 13.91±9.765 | |
| D-Dimers (µg/mL)** | 6.374±2.526 | |
| LDH (U/L)# | 1,053.0±878.9 | |
| Ferritin (ng/mL)& | 2,644±2,057 | |
| Haemoglobin (g/dL) | 12.72±2.152 | |
| Neutrophils (cell/$mm^3$) | 10,000±6,869 | |
| Lymphocytes (cell/$mm^3$) | 1,780±1,219 | |
| Platelets (count/$mm^3$) | 207,400±122,814 | |
| **Medications** | | |
| Antibiotics | 5 | 100% |
| Heparin | 5 | 100% |
| Antimalarial | 0 | 0% |
| Oseltamivir | 2 | 40% |
| Glucocorticoids | 2 | 40% |
| **Respiratory status** | | |
| Mechanical ventilation | 5 | 100% |
| Nasal-cannula oxygen | 5 | 100% |
| Room air | 0 | |
| $pO_2$ | 58.98±15.32 | |
| $SatO_2$ | 85.78±12.57 | |
| **Outcome** | | |
| Deaths | 5 | 100% |

**CRP: C-reactive protein (Normal value <0.5 mg/dL);*
***D-dimers (NV <0.5 µg/mL); #LDH: lactic dehydrogenase (Normal range: 120-246 U/L); &Ferritin (NR: 10-291 ng/mL)*

**Table S6:** Clinical data of twelve patients who died with COVID-19

| **Demographics** | | **%** |
|---|---|---|
| Number | 12 | |
| Age (years) | 50.5±16.45 | |
| Hospital day | 6.5±4.7 | |
| Female | 6 | 50% |
| **Comorbities** | | |
| Hypertension | 7 | 58,3% |
| Diabetes | 2 | 16,6% |
| Obesity | 2 | 16,6% |
| Lung disease | 1 | 8,3% |
| History of smoking | 1 | 8,3% |
| Heart disease | 3 | 25% |
| Kidney disease | 1 | 8,5% |
| Cerebrovascular accident | 0 | 0% |
| Cancer | 3 | 25% |
| Autoimmune diseases | 0 | 0% |
| Vascular diseases | 3 | 25% |
| Immune deficiency | 1 | 8,5% |
| **Outcome** | | |
| Deaths | 12 | 100% |

*[*]CRP: C-reactive protein (Normal value <0.5 mg/dL);*
*[**]D-dimers (NV <0.5 µg/mL); [#]LDH: lactic dehydrogenase (Normal range: 120-246 U/L); [&]Ferritin (NR: 10-291 ng/mL)*

**Table S7:** Clinical data of patients controls

| **Demographics** | | **%** |
|---|---|---|
| Number | 8 | |
| Age (years) | 63.6±15.5 | |
| Male | 6 | 75% |
| Female | 2 | 25% |
| **Cause of death** | | |
| Heart infarction | 6 | 75% |
| Cardiopulmonary insufficiency | 1 | 12.5% |
| Lung embolism | 1 | 12.5% |

## SI References


1. D. D. S. Garcia, *et al.*, Anxiety and depression symptoms disrupt resting state connectivity in patients with genetic generalized epilepsies. *Epilepsia* **60**, 679–688 (2019).

2. D. Wechsler, Wechsler Memory Scale-Revised. *Psychological Corporation* (1987) (April 28, 2022).

3. K. R. Campanholo, *et al.*, Performance of an adult Brazilian sample on the Trail Making Test and Stroop Test. *Dement Neuropsychol* **8**, 26–31 (2014).

4. E. Strauss, *et al.*, *A Compendium of Neuropsychological Tests: Administration, Norms, and Commentary* (Oxford University Press, 2006).

5. C. Jackson, The Chalder Fatigue Scale (CFQ 11). *Occup. Med.* **65**, 86 (2015).

6. A. N. Bertolazi, *et al.*, Portuguese-language version of the Epworth sleepiness scale: validation for use in Brazil. *Jornal Brasileiro de Pneumologia* **35**, 877–883 (2009).

7. R. C. Team, 2020. *R: A Language and Environment for Statistical Computing. R Foundation for Statistical Computing, Vienna, Austria: Available at: https://www. R-project. org/. [Google Scholar]* (2019).

8. K. L. Grasby, *et al.*, The genetic architecture of the human cerebral cortex. *Science* **367** (2020).

9. R. Righart, *et al.*, Volume versus surface-based cortical thickness measurements: A comparative study with healthy controls and multiple sclerosis patients. *PLoS One* **12**, e0179590 (2017).

10. R. S. Desikan, *et al.*, An automated labeling system for subdividing the human cerebral cortex on MRI scans into gyral based regions of interest. *Neuroimage* **31**, 968–980 (2006).

11. Y. Bol, A. A. Duits, R. M. M. Hupperts, I. Verlinden, F. R. J. Verhey, The impact of fatigue on cognitive functioning in patients with multiple sclerosis. *Clin. Rehabil.* **24**, 854–862 (2010).

12. B. Pinto, *et al.*, Fatigue and its correlates in Indian patients with systemic lupus erythematosus. *Clin. Rheumatol.* **40**, 905–911 (2021).

13. Y. Benjamini, Y. Hochberg, Controlling the False Discovery Rate: A Practical and Powerful Approach to Multiple Testing. *Journal of the Royal Statistical Society: Series B (Methodological)* **57**, 289–300 (1995).

14. A. M. Fraga, *et al.*, Establishment of a Brazilian Line of Human Embryonic Stem Cells in Defined Medium: Implications for Cell Therapy in an Ethnically Diverse Population. *Cell Transplant.* **20**, 431–440 (2011).

15. P. Trindade, *et al.*, Short and long TNF-alpha exposure recapitulates canonical astrogliosis events in human-induced pluripotent stem cells-derived astrocytes. *Glia* **68**, 1396–1409 (2020).

16. P. F. Ledur, *et al.*, Zika virus infection leads to mitochondrial failure, oxidative stress and DNA damage in human iPSC-derived astrocytes. *Sci. Rep.* **10**, 1218 (2020).

17. Y. Yan, *et al.*, Efficient and rapid derivation of primitive neural stem cells and generation of brain subtype neurons from human pluripotent stem cells. *Stem Cells Transl. Med.* **2**, 862–870 (2013).

18. J. B. Case, *et al.*, Neutralizing Antibody and Soluble ACE2 Inhibition of a Replication-Competent VSV-SARS-CoV-2 and a Clinical Isolate of SARS-CoV-2. *Cell Host Microbe* **28**, 475–485.e5 (2020).

19. A. C. Yang, *et al.*, Dysregulation of brain and choroid plexus cell types in severe COVID-19. *Nature*

**595**, 565–571 (2021).

20. T. Stuart, *et al.*, Comprehensive Integration of Single-Cell Data. *Cell* **177**, 1888–1902.e21 (2019).

21. C. A. Schneider, W. S. Rasband, K. W. Eliceiri, NIH Image to ImageJ: 25 years of image analysis. *Nat. Methods* **9**, 671–675 (2012).

22. N. D. Mendes, *et al.*, Free-floating adult human brain-derived slice cultures as a model to study the neuronal impact of Alzheimer's disease-associated Aβ oligomers. *J. Neurosci. Methods* **307**, 203–209 (2018).

23. A. Fernandes, *et al.*, Short-Term Free-Floating Slice Cultures from the Adult Human Brain. *J. Vis. Exp.* (2019) https:/doi.org/10.3791/59845.

24. U. Distler, J. Kuharev, P. Navarro, S. Tenzer, Label-free quantification in ion mobility–enhanced data-independent acquisition proteomics. *Nat. Protoc.* **11**, 795–812 (2016).

25. P. Shannon, *et al.*, Cytoscape: a software environment for integrated models of biomolecular interaction networks. *Genome Res.* **13**, 2498–2504 (2003).

26. G. Yu, L.-G. Wang, Y. Han, Q.-Y. He, clusterProfiler: an R package for comparing biological themes among gene clusters. *OMICS* **16**, 284–287 (2012).

27. X. Zhang, *et al.*, CellMarker: a manually curated resource of cell markers in human and mouse. *Nucleic Acids Res.* **47**, D721–D728 (2019).

28. M. Kanehisa, S. Goto, KEGG: kyoto encyclopedia of genes and genomes. *Nucleic Acids Res.* **28**, 27–30 (2000).

29. G. Wu, X. Feng, L. Stein, A human functional protein interaction network and its application to cancer data analysis. *Genome Biol.* **11**, R53 (2010).

30. A. C. Schrimpe-Rutledge, S. G. Codreanu, S. D. Sherrod, J. A. McLean, Untargeted Metabolomics Strategies-Challenges and Emerging Directions. *J. Am. Soc. Mass Spectrom.* **27**, 1897–1905 (2016).

31. T. D. Schmittgen, K. J. Livak, Analyzing real-time PCR data by the comparative C(T) method. *Nat. Protoc.* **3**, 1101–1108 (2008).

32. J. Won, *et al.*, Development of a Laboratory-safe and Low-cost Detection Protocol for SARS-CoV-2 of the Coronavirus Disease 2019 (COVID-19). *Exp. Neurobiol.* **29**, 107–119 (2020).

33. A. C. Codo, *et al.*, Elevated Glucose Levels Favor SARS-CoV-2 Infection and Monocyte Response through a HIF-1α/Glycolysis-Dependent Axis. *Cell Metab.* (2020) https:/doi.org/10.1016/j.cmet.2020.07.007.

34. M. M. Shipley, C. A. Mangold, M. L. Szpara, Differentiation of the SH-SY5Y Human Neuroblastoma Cell Line. *J. Vis. Exp.*, 53193 (2016).

35. H. Xicoy, B. Wieringa, G. J. M. Martens, The SH-SY5Y cell line in Parkinson's disease research: a systematic review. *Molecular Neurodegeneration* **12** (2017).

36. J. Kovalevich, D. Langford, Considerations for the use of SH-SY5Y neuroblastoma cells in neurobiology. *Methods Mol. Biol.* **1078**, 9–21 (2013).

37. G. J. Brewer, Serum-free B27/neurobasal medium supports differentiated growth of neurons from the striatum, substantia nigra, septum, cerebral cortex, cerebellum, and dentate gyrus. *Journal of Neuroscience Research* **42**, 674–683 (1995).

38. C. A. Trujillo, *et al.*, Novel perspectives of neural stem cell differentiation: from neurotransmitters to therapeutics. *Cytometry A* **75**, 38–53 (2009).

39. Y. Elkabetz, L. Studer, Human ESC-derived neural rosettes and neural stem cell progression. *Cold Spring Harb. Symp. Quant. Biol.* **73**, 377–387 (2008).

40. B. S. Casas, *et al.*, hiPSC-derived neural stem cells from patients with schizophrenia induce an impaired angiogenesis. *Transl. Psychiatry* **8**, 48 (2018).

41. J. A. White 2nd, *et al.*, Excess Rab4 rescues synaptic and behavioral dysfunction caused by defective HTT-Rab4 axonal transport in Huntington's disease. *Acta Neuropathol Commun* **8**, 97 (2020).

42. L. Goto-Silva, *et al.*, Computational fluid dynamic analysis of physical forces playing a role in brain organoid cultures in two different multiplex platforms. *BMC Dev. Biol.* **19**, 3 (2019).

43. Y. Perez-Riverol, *et al.*, The PRIDE database and related tools and resources in 2019: improving support for quantification data. *Nucleic Acids Research* **47**, D442–D450 (2019).